J. Fluid Mech. (1994), *vol.* 265, *pp.* 161–188

The collision rate of small drops in linear flow fields

By HUA WANG, ALEXANDER Z. ZINCHENKO AND ROBERT H. DAVIS†

Department of Chemical Engineering, University of Colorado, Boulder, CO 80309-0424, USA

(Received 30 July 1993 and in revised form 1 October 1993)

A dilute dispersion containing small, force-free drops of one fluid dispersed in a second, immiscible fluid in a linear flow field is considered for small Reynolds numbers and large Péclet numbers under isothermal conditions. The emphasis of our analysis is on the effects of pairwise drop interactions on their collision rate, as described by the collision efficiency, using a trajectory analysis. Simple shear flow and uniaxial extensional or compressional flow are considered. For both flows, the collision efficiency decreases with increasing drop viscosity due to the effects of hydrodynamic interactions. It also decreases as the ratio of the smaller drop radius to the larger radius decreases. For uniaxial flow, finite collision rates are predicted in the absence of interdroplet forces for all finite values of the drop size ratio and the ratio of the viscosities of the drop and suspending medium. In contrast, several kinds of relative trajectories exist for a pair of drops in simple shear flow, including open trajectories, collision trajectories, and closed and semi-closed trajectories, in the absence of interdroplet forces. When the ratio of small to large drop diameters is smaller than a critical value, which increases with increasing drop viscosity, all of the relative trajectories that start with the two drops far apart remain open (no collisions), unless in the presence of attractive forces. Attractive van der Waals forces are shown to increase the collision rates.

1. Introduction

Collisions and coalescence of small drops dispersed in another liquid or a gas play important roles in a wide variety of natural and industrial processes, such as raindrop growth, liquid–liquid extraction, and the processing of liquid-phase miscibility gap materials. Collision and coagulation of solid particles induced by Brownian motion and gravity sedimentation have been investigated intensively for small Reynolds numbers. For rigid spheres with simultaneous effects of hydrodynamic interactions and interparticle attractive and repulsive forces, Spielman (1970), Valioulis & List (1984), and Kim & Zukoski (1990) extended the classic work of Smoluchowski (1917) by solving the steady-state diffusion equation describing the relative Brownian motion between two coagulating particles. For gravity-induced coagulation of rigid spheres, theoretical models have been developed by Davis (1984) and Merik & Fogler (1984) to predict the rate of coagulation using trajectory analyses, and by Wen & Batchelor (1985) using an asymptotic method for solving the Fokker–Planck pair conservation equation. Recently, these analyses have been extended to predict the collision rate of

† To whom correspondence should be addressed.

two interacting spherical fluid drops induced by Brownian motion, gravity sedimentation and thermocapillary migration (Zhang & Davis 1991, 1992; Satrape 1992; Wang & Davis 1993; Zhang, Wang & Davis 1993).

In the works cited above, the dispersions are assumed to be quiescent (no stirring or imposed flow), other than as a result of the motion of individual drops. Smoluchowski (1917) made the first attempt to estimate the rate of coagulation in a dilute dispersion of rigid spheres in a shear flow. In his classical model, the spheres are assumed to move independently, without any hydrodynamic interactions or interparticle attractive and repulsive forces other than a sticking force upon contact. Accounting for the effects of hydrodynamic interactions and interparticle attractive force, Curtis & Hocking (1970) applied their calculations to experiments on coagulation in simple shear flow to estimate the Hamaker constant. Batchelor & Green (1972*a*, *b*) obtained the general form of hydrodynamic interaction between a pair of particles in a linear flow field. They also complemented the bispherical-coordinate solution of Lin, Lee & Sather (1970) with near- and far-field asymptotic expressions for hydrodynamic functions. Van de Ven & Mason (1976) and Zeichner & Schowalter (1977) combined the general approach of Batchelor & Green (1972*a*) and DLVO (Derjaguin & Landau 1941; Verway & Overbeek 1948) theory to predict the coagulation rate for monodispersed rigid spheres in the shear fields. Later, the relative motion and collisions of unequal-sized particles were analysed by Adler (1981). The effect of weak bulk convection on the Brownian collisions is discussed by van de Ven & Mason (1977), and the effect of weak Brownian diffusion on shear-induced coagulation of colloidal dispersions was considered by Feke & Schowalter (1983). In the current work, we predict collision rates for small, freely suspended spherical fluid drops which are subjected to prescribed bulk shear flows.

It is well known that lubrication forces prevent rigid particles with smooth surfaces from coming into physical contact in the absence of an attractive force that increases as the separation distance decreases. In contrast, when drops approach each other in near contact, the mobility of their interfaces allows the fluid between them to be squeezed outward with much less resistance than for the case of rigid particles. As discussed by Davis, Schonberg & Rallison (1989), this allows for non-zero collision rates of non-deforming drops, even in the absence of attractive forces. However, there are only few studies of the coalescence of fluid drops in a shear flow field, presumably because of the more complex interactions which involve fluid flow both inside and outside the drops and which include the possibility that the drops will deform as they collide. Zinchenko (1983) calculated the hydrodynamic interactions between a pair of equal-sized, non-deforming drops in a linear flow field. Later, Zinchenko (1984) used this solution to analyse the rheological properties of dilute emulsions. To the best of our knowledge, the collision rate of two arbitrary-sized drops in a shear flow has not been studied before.

The present work employs the complete solutions for hydrodynamic interactions of two spherical drops in a linear flow field to calculate the collision rate by extending the previous work for rigid particles. In §2, the effects of drop interactions on their relative motion are discussed. The hydrodynamic interactions are presented as two-sphere relative mobility functions, with the details of the calculation of relative mobility functions presented in Appendices A and B. In §3, theoretical models for shear-induced collision rates are developed. The analysis is limited to large Péclet numbers so that Brownian motion can be neglected. In §4, a trajectory analysis is used to determine the collision rates in the two prototype flows, namely steady uniaxial extensional (pure stretching) flow and steady simple shear flow. The results of numerical computations

for collision efficiencies are presented and discussed. Concluding remarks are given in §5.

2. Interaction between spherical drops

2.1. *Expression for the relative velocity of two drops*

A dilute dispersion containing spherical drops of viscosity μ' dispersed in an immiscible fluid of viscosity μ is considered. Both fluids are Newtonian and isothermal, and it is assumed that there are no surfactants on the drop surface. For dilute dispersions, the probability of a third drop influencing the relative motion of two interacting drops is small, and so the analysis is restricted to binary interactions of drops of radii a_1 (large drop) and a_2 (small drop). The drops are of such small sizes that they remain spherical (small capillary number), and that inertia may be neglected (small Reynolds number). The ambient flow field has velocity $\boldsymbol{U}^{(0)}(\boldsymbol{x}, t)$, which is assumed to be a linear function of position and can therefore be characterized instantaneously by a uniform rate-of-strain tensor,

$$\boldsymbol{E} = \tfrac{1}{2}[(\nabla \boldsymbol{U}^{(0)}) + (\nabla \boldsymbol{U}^{(0)})^T], \tag{1}$$

and a rigid-body rotation with constant angular velocity,

$$\boldsymbol{\Omega} = \tfrac{1}{2}\nabla \times \boldsymbol{U}^{(0)}. \tag{2}$$

Because of the linearity of the creeping flow equations, the velocity field can be decomposed into velocity caused by the motion of force-free drops and that caused by the interdroplet forces. Moreover, the relative velocity can be decomposed into motion along and normal to the line-of-centres of the two drops (Batchelor & Green 1972*a*):

$$\boldsymbol{V}_{12}(\boldsymbol{r}) = \boldsymbol{\Omega} \times \boldsymbol{r} + \boldsymbol{E} \cdot \boldsymbol{r} - \left[\mathscr{A}(s)\frac{\boldsymbol{rr}}{r^2} + \mathscr{B}(s)\left(\boldsymbol{I} - \frac{\boldsymbol{rr}}{r^2}\right)\right] \cdot \boldsymbol{E} \cdot \boldsymbol{r} - \frac{D_{12}^{(0)}}{kT}\left[\frac{\boldsymbol{rr}}{r^2}\mathscr{G}(s) + \left(\boldsymbol{I} - \frac{\boldsymbol{rr}}{r^2}\right)\mathscr{H}(s)\right] \cdot \nabla(\Phi_{12}), \tag{3}$$

where $\boldsymbol{r}$ is the vector from the centre of drop 1 to the centre of drop 2, $\boldsymbol{I}$ is the unit second-order tensor, and $s = 2r/(a_1 + a_2)$ is the dimensionless centre-to-centre distance. The relative diffusivity due to Brownian motion for two widely separated drops is

$$D_{12}^{(0)} = \frac{kT(\hat{\mu}+1)(1+\lambda^{-1})}{2\pi\mu(3\hat{\mu}+2)a_1}, \tag{4}$$

where $\hat{\mu} = \mu'/\mu$ is the viscosity ratio, $\lambda = a_2/a_1$ is the radius ratio, $k = 1.381 \times 10^{-16}$ erg K^{-1} is the Boltzmann constant, and T is the absolute temperature.

The interdroplet force is given by $-\nabla\Phi_{12}$. The total interdroplet potential, Φ_{12}, is usually assumed to be the sum of the individual attractive and repulsive contributions by the DLVO theory (Derjaguin & Landau 1941; Verway & Overbeek 1948). It is assumed here that the drop interfaces are clean and do not carry any repulsive charges. Then, the interparticle force is attractive and results from London–van der Waals induced-dipole interactions. The van der Waals potential as a function of drop separation was first calculated by Hamaker (1937) using a pairwise additivity theory. For unequal-sized spheres without retardation, the force potential as a function of the drop separation is

$$\Phi_{12} = -\frac{A}{6}\left\{\frac{8\lambda}{(s^2-4)(1+\lambda)^2} + \frac{8\lambda}{s^2(1+\lambda)^2 - 4(1-\lambda)^2} + \ln\left[\frac{(s^2-4)(1+\lambda)^2}{s^2(1+\lambda)^2 - 4(1-\lambda)^2}\right]\right\}, \tag{5}$$

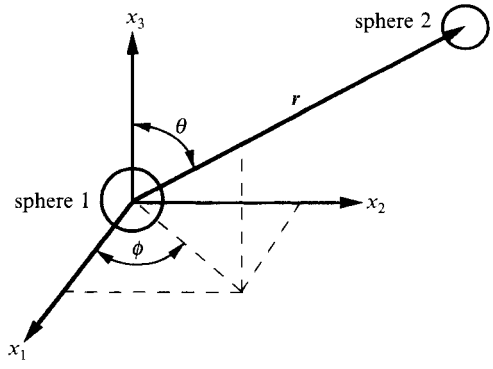

FIGURE 1. Schematic of the coordinate system used for trajectory equations.

where A is the composite Hamaker constant, which is typically of order 10^{-19}–10^{-21} J (Russel, Saville & Schowalter 1989).

The relative trajectory of a pair of drops is needed for determination of the flow-induced collision rate. The trajectories are described in the coordinate system as shown in figure 1. For simple shear flow having the ambient flow velocity components $(\gamma x_2, 0, 0)$, carrying out the vector and tensor operations indicated by (3) yields the dimensionless trajectory equations

$$\frac{\mathrm{d}s}{\mathrm{d}\tau} = (1-\mathscr{A})\, s \sin^2\theta \sin\phi\cos\phi - \frac{\mathscr{G}}{Q_{12}}\frac{\mathrm{d}\phi_{12}}{\mathrm{d}s}, \tag{6}$$

$$\frac{\mathrm{d}\phi}{\mathrm{d}\tau} = -\sin^2\phi - \tfrac{1}{2}\mathscr{B}(\cos^2\phi - \sin^2\phi), \tag{7}$$

$$\frac{\mathrm{d}\theta}{\mathrm{d}\tau} = (1-\mathscr{B})\sin\theta\cos\theta\sin\phi\cos\phi, \tag{8}$$

where $\tau = \gamma t$ is the dimensionless time, $\phi_{12} = \Phi_{12}/A$ is the dimensionless interdroplet potential scaled with the Hamaker constant, and Q_{12} is the dimensionless interparticle force which measures the relative importance of ambient flow to the van der Waals attraction:

$$Q_{12} \equiv \frac{\frac{1}{4}a_1^2(1+\lambda)^2\gamma}{AD_{12}^0/kT}. \tag{9}$$

Note that Q_{12} is proportional to the third power of the drop radius. Thus, the contribution of the van der Waals attraction to the drop relative motion is small for large drops, except when the drops are very close to one another.

For pure straining flows, namely uniaxial extensional flow with the velocity components $(-\gamma x_1, -\gamma x_2, 2\gamma x_3)$, and uniaxial compressional flow, which is the reverse of the extensional flow, carrying out the vector and tensor operations indicated by (3) yields the dimensionless trajectory equations

$$\frac{\mathrm{d}s}{\mathrm{d}\tau} = \pm(1-\mathscr{A})\, s(3\cos^2\theta - 1) - \frac{\mathscr{G}}{Q_{12}}\frac{\mathrm{d}\phi_{12}}{\mathrm{d}s}, \tag{10}$$

$$\frac{\mathrm{d}\theta}{\mathrm{d}\tau} = \mp\, 3(1-\mathscr{B})\sin\theta\cos\theta, \tag{11}$$

$$\frac{\mathrm{d}\phi}{\mathrm{d}\tau} = 0, \tag{12}$$

where the upper and lower signs correspond to uniaxial extensional flow and compressional flow, respectively.

2.2. *Mobility functions for the relative motion of two drops*

The relative mobility functions of drop motion along the line-of-centres ($\mathscr{A}$ and $\mathscr{G}$) and motion normal to the line-of-centres ($\mathscr{B}$ and $\mathscr{H}$) describe the effects of hydrodynamic interactions between two spherical drops. These functions depend on the size ratio of the two drops, λ, the drop-to-medium viscosity ratio, $\hat{\mu}$, and the dimensionless distance between the drops, $s = 2r/(a_1+a_2)$, and they are unchanged when λ is replaced with λ^{-1}. Complete analytical and numerical results for the relative mobility $\mathscr{G}$ for arbitrary separation have been presented previously by Zhang & Davis (1991). For hydrodynamic interactions of two widely separated drops in a linear flow field, the relative mobility functions $\mathscr{A}$ and $\mathscr{B}$ can be obtained using a method of reflections similar to that employed by Batchelor & Green (1972*a*) for solid particles, yielding

$$\mathscr{A}(s) = 4\frac{(2+5\hat{\mu})(1+\lambda^3)}{(1+\hat{\mu})(1+\lambda)^3}\frac{1}{s^3} - 48\frac{\hat{\mu}(2+3\hat{\mu})(1+\lambda^5)+\hat{\mu}(2+5\hat{\mu})\lambda^2(1+\lambda)}{(1+\hat{\mu})(2+3\hat{\mu})(1+\lambda)^5}\frac{1}{s^5} + O\left(\frac{1}{s^8}\right), \quad (13)$$

and

$$\mathscr{B}(s) = 32\frac{\hat{\mu}(2+3\hat{\mu})(1+\lambda^5)+\hat{\mu}(2+5\hat{\mu})\lambda^2(1+\lambda)}{(1+\hat{\mu})(2+3\hat{\mu})(1+\lambda)^5}\frac{1}{s^5} + O\left(\frac{1}{s^6}\right). \quad (14)$$

In the case of equal-sized drops, these relations agree with the far-field asymptotics of Zinchenko (1983). According to (14), for the bubble case ($\hat{\mu} = 0$), the leading term of the function $\mathscr{B}$ vanishes. Interestingly, it can be proved that, when $\hat{\mu} = 0$, the function $\mathscr{B}$ is identically zero for all separations.

The far-field expressions (13) and (14) are valid only when the separation between the two drops is large compared to their radii a_1 and a_2. Less restrictive, analytical expressions for $\mathscr{A}$ and $\mathscr{B}$, valid for separations large compared to the smaller radius a_2, may be obtained by image techniques (Fuentes, Kim & Jeffrey 1988, 1989). For our coalescence problem, the range $r-a_1-a_2 < a_2$ is of primary importance, and so the more comprehensive, exact bispherical-coordinate solutions for two arbitrary-sized drops in a linear flow field are used in the present work. When the dimensionless gap separation, $\xi \equiv s-2$, between two drops is small, the convergence of series solutions becomes poor, and so the asymptotic results of Zinchenko (1982) and Davis *et al.* (1989) are used to calculate the near-field interaction (see Appendices A and B for details of the hydrodynamic functions).

Typical results for the relative mobility functions along the line-of-centres, $\mathscr{A}$, and normal to the line-of-centres, $\mathscr{B}$, as functions of the dimensionless distance between two drop surfaces, ξ, are plotted in figures 2 and 3 for drops with size ratio $\lambda = 0.2$, 0.5, and 1.0, and various viscosity ratios. In these figures, the far-field asymptotic expansions and the near-field approximate expansions are represented by long-dashed lines and short-dashed lines, respectively, and the corresponding results from the exact bispherical-coordinates solutions are shown as solid lines for comparison. The far-field expansions for $\mathscr{A}$ and $\mathscr{B}$ are accurate to within a few percent for separations as small as one-half of the average drop radius. In fact, the far-field expansions for $\mathscr{B}$ may be used for all separations when $\hat{\mu} \leqslant 0.1$. The near-field expansions for $\mathscr{A}$, and for $\mathscr{B}$ with low $\hat{\mu}$, are accurate to within a few percent for dimensionless separations less than 1×10^{-2}. For drops with high viscosity ratios, the near-field asymptotics for $\mathscr{B}$ are accurate only for values of ξ less than about 3×10^{-4}. The mobility functions increase with increasing viscosity ratio, indicating stronger hydrodynamic interactions. For

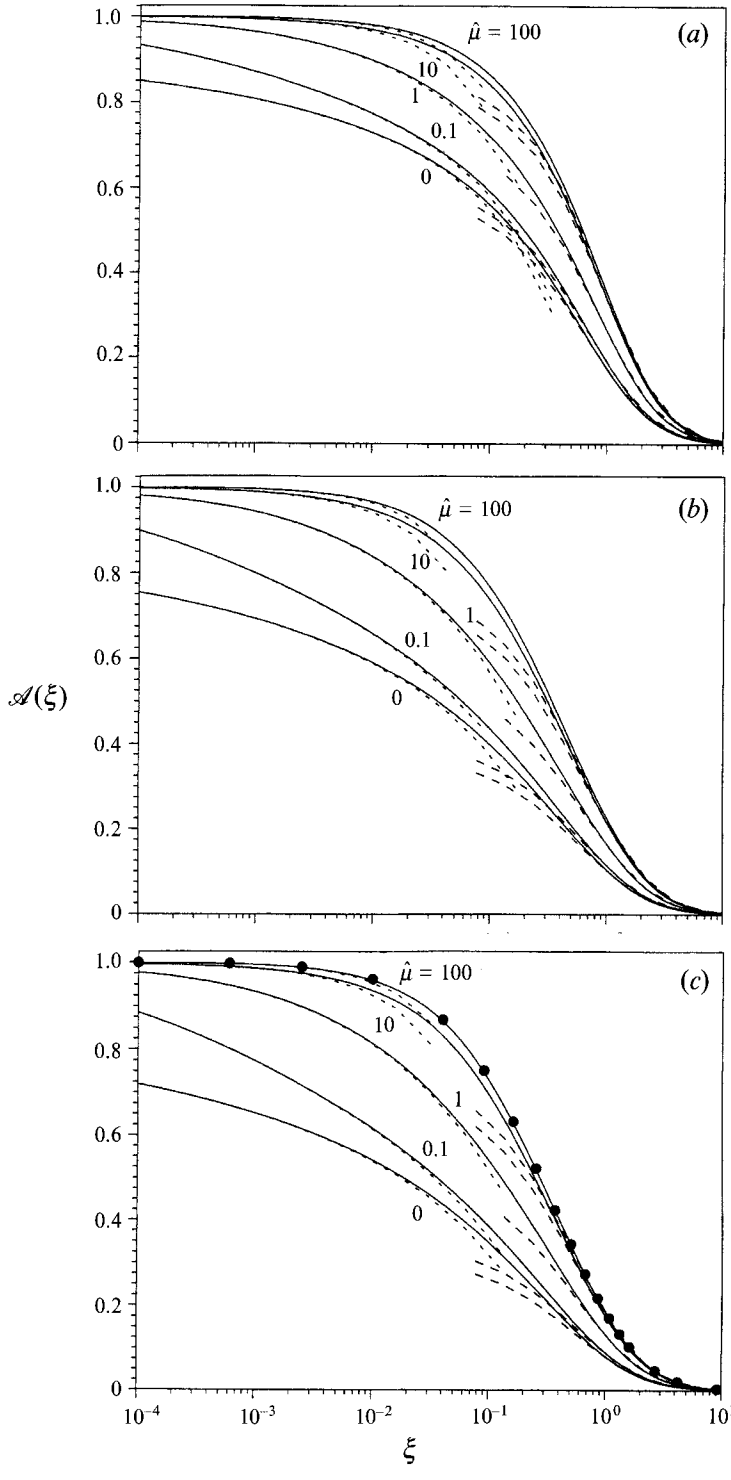

FIGURE 2. The relative mobility function $\mathscr{A}$ along the line-of-centres as a function of the dimensionless distance between two drop surfaces with different viscosity ratios $\hat{\mu}$ for size ratios (*a*) $\lambda = 0.2$, (*b*) $\lambda = 0.5$, and (*c*) $\lambda = 1.0$. The solid lines are from the bispherical-coordinate solution; the long and short dashed lines are the far-field and near-field asymptotic expressions, respectively. The solid circles for $\lambda = 1$ are the rigid-sphere results of Batchelor & Green (1972*a*).

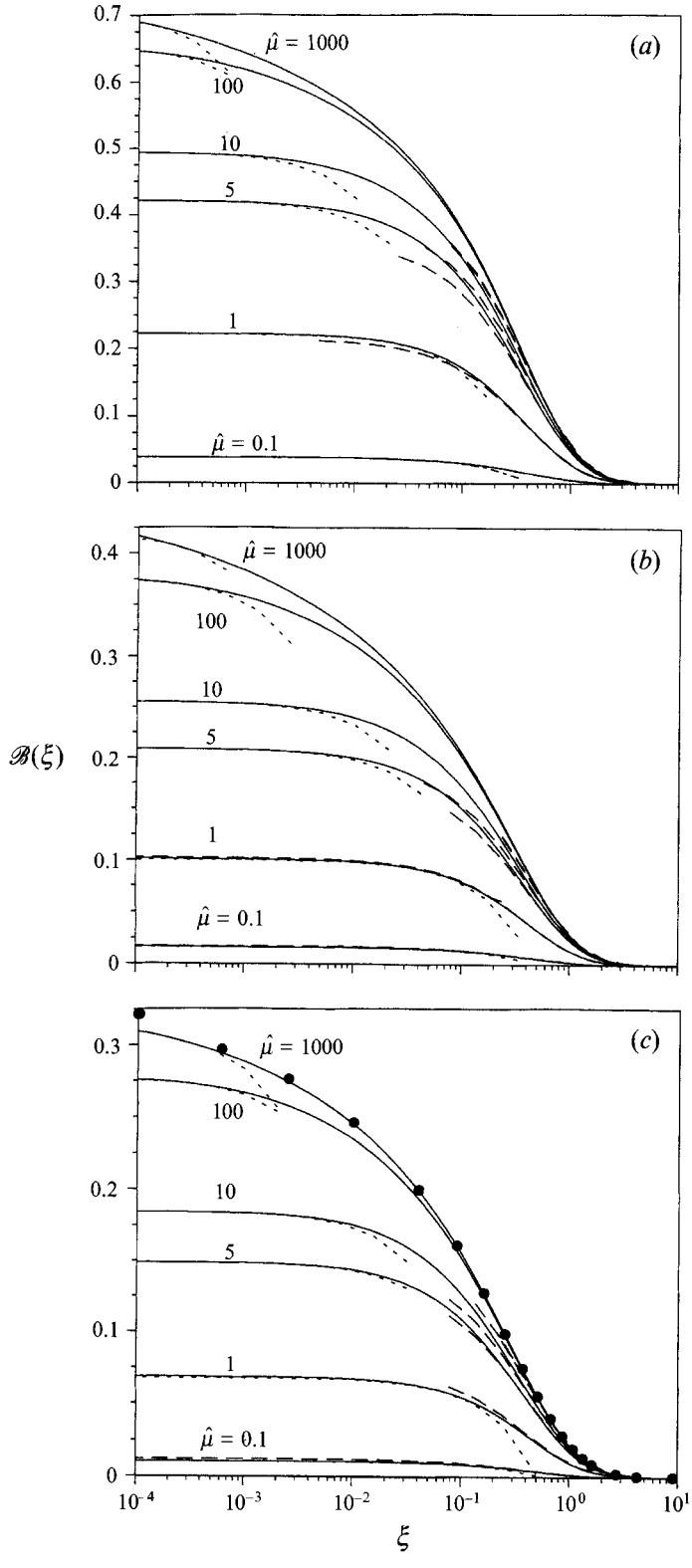

FIGURE 3. As figure 2 but for the relative mobility function $\mathscr{B}$ normal to the line-of-centres.

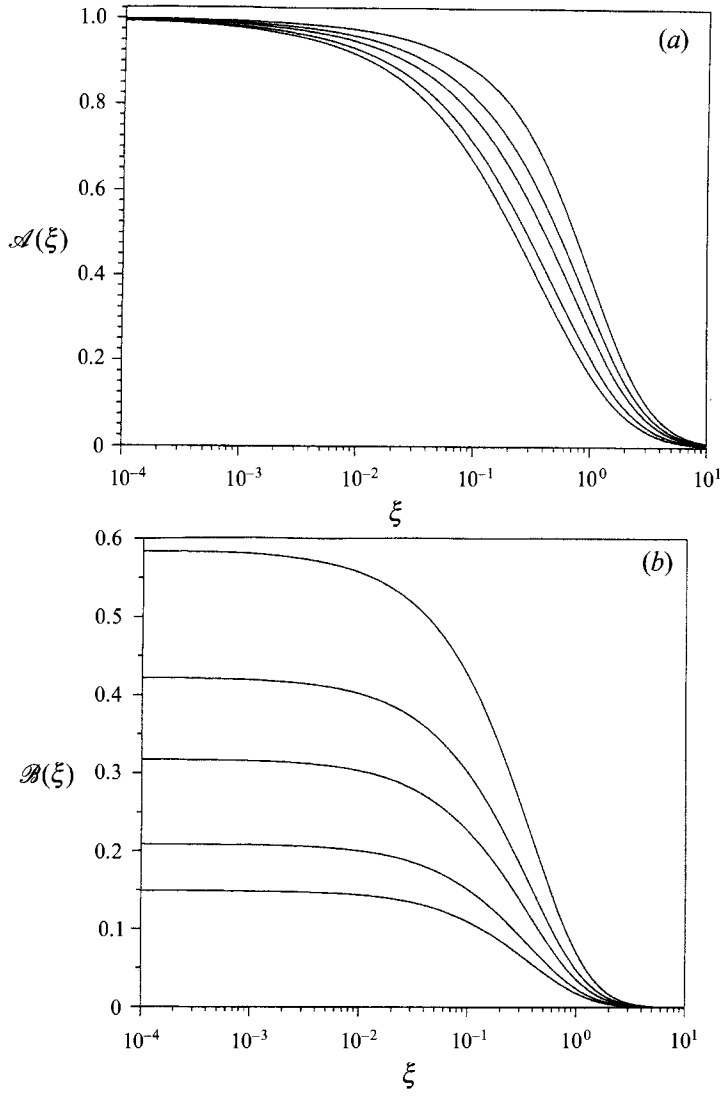

FIGURE 4. The relative mobility functions (*a*) along to the line-of-centres, $\mathscr{A}$, and (*b*) normal to the line-of-centres, $\mathscr{B}$, as functions of the dimensionless distance between two drop surfaces for a viscosity ratio $\hat{\mu} = 5.0$, with different size ratios, $\lambda = 1.0$, 0.5, 0.3, 0.2, and 0.1, respectively, from left to right.

large viscosity ratios ($\hat{\mu} \geqslant 100$), the present results are in close agreement with the previous results by Batchelor & Green (1972*a*) for rigid spheres, except for the function $\mathscr{B}$ at very small separations.

Figure 4 shows the influence of the size ratio on the mobility functions. It is noted that the mobility functions $\mathscr{A}$ and $\mathscr{B}$ increase with drop size ratio decreasing. This is because a small drop tends to flow along the streamlines surrounding a large drop when the size ratio is small, therefore resulting in a highly disturbed motion of the small drop and thus strong hydrodynamic interactions and large mobility functions $\mathscr{A}$ and $\mathscr{B}$.

3. Expressions for the drop collision rate

The rate at which the drops of radius a_1 collide with the drops of radius a_2 per unit volume is equal to the flux of pairs into the contact surface $r = a_1 + a_2$ and is expressed in terms of the pair-distributed function $p_{12}(\boldsymbol{r})$ and the drop relative velocity $\boldsymbol{V}_{12}$, as given by Davis (1984),

$$J_{12} = -n_1 n_2 \int_{r=a_1+a_2} p_{12}\, \boldsymbol{V}_{12} \cdot \boldsymbol{n}\, \mathrm{d}A, \tag{15}$$

where $\boldsymbol{n} = \boldsymbol{r}/r$ is the outward unit normal to the spherical contact surface represented by $r = a_1 + a_2$, and n_1 and n_2 are the number of drops at the given time in the size categories characterized by radius a_1 and radius a_2, respectively, per unit volume of the dispersion.

For a dilute dispersion, the pair distribution is governed by the quasi-steady mass conservation equation for regions of space outside the contact surface,

$$\nabla \cdot (p_{12}\, \boldsymbol{V}_{12}) = 0. \tag{16}$$

The upstream boundary condition is $p_{12} \to 1$ as $r \to \infty$.

For supramicron drops having high Péclet numbers, the relative motion of two drops of different size is deterministic, and the collision rate may be found using a trajectory analysis. Using (16) and the divergence theorem, the integral in (15) can be taken over the surface that encloses the volume occupied by all trajectories that originate at $r = \infty$ and terminate with the drops coming into contact. The collision rate then must equal the flux at $r = \infty$ though a cross-section A_c, to be referred as the upstream interception area. As $r \to \infty$, $p_{12} \to 1$, and $\boldsymbol{V}_{12} \to \boldsymbol{U}_{12}^{(0)} = \boldsymbol{\Omega} \times \boldsymbol{r} + \boldsymbol{E} \cdot \boldsymbol{r}$, and so the collision efficiency can be determined through an upstream interception area A_c by

$$J_{12} = -n_1 n_2 \int_{A_c} \boldsymbol{U}_{12}^{(0)} \cdot \boldsymbol{n}\, \mathrm{d}S. \tag{17}$$

When hydrodynamic and interdroplet interactions are neglected up to the instant of contact, as in Smoluchowski's model, the particle trajectories coincide with the undisturbed streamlines of the bulk motion. These streamlines are straight lines in simple shear flow. In this case, the boundary of A_c is then a circle of radius $a_1 + a_2$. The collision rate is (Smoluckowski 1917)

$$J_{12}^{(0)} = \tfrac{4}{3} n_1 n_2 \gamma (a_1 + a_2)^3. \tag{18}$$

For uniaxial extensional or compressional flow without hydrodynamic and interdroplet interactions, the collision rate is (Zeichner & Schowalter 1977):

$$J_{12}^{(0)} = \frac{8\pi}{3\sqrt{3}} n_1 n_2 \gamma (a_1 + a_2)^3. \tag{19}$$

The collision efficiency is defined as the ratio of the collision rate in the presence of interactions to that in their absence:

$$E_{12} \equiv J_{12}/J_{12}^{(0)}. \tag{20}$$

The upstream interception area, which defines the area within which two widely separated drops will eventually collide and coalesce, may be determined by a trajectory analysis which includes hydrodynamic and interdroplet interactions. The details of the trajectory analysis, both with without van der Waals attractions, are discussed in the following section.

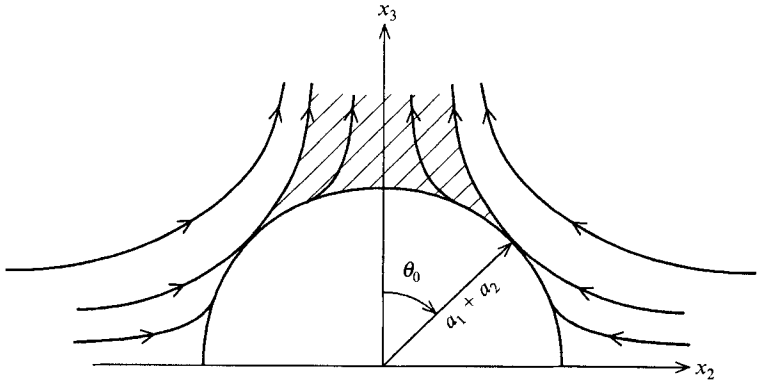

FIGURE 5. Pattern of the relative trajectories in the $(\bar{x}_2, \bar{x}_3)$ half-plane for drops in a uniaxial extensional flow field. The three-dimensional aspect of these trajectories is obtained by rotating the depicted pattern about the $\bar{x}_3$ axis through 360°.

4. Results and discussion

4.1. *Drop collisions in uniaxial extensional flow without interdroplet forces*

In uniaxial extensional flow, the pattern of relative trajectories in the (x_2, x_3)-half-plane is shown in figure 5. The relative trajectories are symmetrical about the x_3 axis and the plane $x_3 = 0$. In the absence of van der Waals forces, the relative trajectories are determined by dividing (10) by (11) and integrating to yield

$$s^3 \sin^2\theta \cos\theta = C\varphi^3(s), \tag{21}$$

where C is the constant specifying a particular trajectory, and the function $\varphi(s)$ is given by

$$\varphi(s) = \exp\left[\int_s^\infty \frac{\mathscr{A}(s') - \mathscr{B}(s')}{1 - \mathscr{A}(s')} \frac{\mathrm{d}s'}{s'}\right]. \tag{22}$$

Following the work of Zinchenko (1984), it is seen that, when

$$|C| > C_{cr} = 16/(3\sqrt{3}\varphi^3(2)),$$

the corresponding trajectories arrive from infinity and return to infinity without reaching the contact sphere $s = 2$. There are also trajectories arriving from infinity at the contact sphere $s = 2$ when $|C| < C_{cr}$. The critical trajectories with $C = \pm C_{cr}$ touch the sphere $s = 2$ at $\theta = \theta_0$ or at $\pi - \theta_0$, where $\theta_0 = \arctan\sqrt{2}$. The direction of the trajectories reverses for the case of uniaxial compressional flow.

The pair distribution function in the shaded region in figure 5 equals zero at steady state. Following the analysis by Batchelor & Green (1972*b*) and Zinchenko (1984), the pair distribution function in the remaining part of $\boldsymbol{r}$-space can be found by the Liouville equation:

$$\nabla\cdot(p_{12}\boldsymbol{V}_{12}) = q_{12}\boldsymbol{V}_{12}\cdot\nabla(p_{12}/q_{12}) = 0, \tag{23}$$

where

$$q_{12} = (1 - \mathscr{A})^{-1}\varphi^{-3}(s). \tag{24}$$

Thus we find that $p_{12}(\boldsymbol{r}) \equiv q_{12}(\boldsymbol{r})$ everywhere with $s > 2$, except in the shaded region. Substituting (24) for $p_{12}(\boldsymbol{r})$ into the definition (15) of the collision rate, we have

$$J_{12} = \frac{8\pi}{3\sqrt{3}\varphi^3(2)} n_1 n_2 (a_1 + a_2)^3. \tag{25}$$

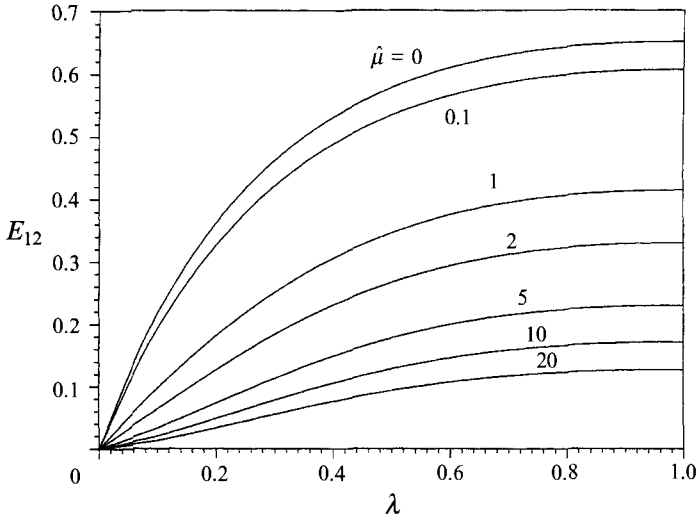

FIGURE 6. The collision efficiency for drops in uniaxial flow as a function of the size ratio λ for different viscosity ratios $\hat{\mu}$ without interdroplet forces.

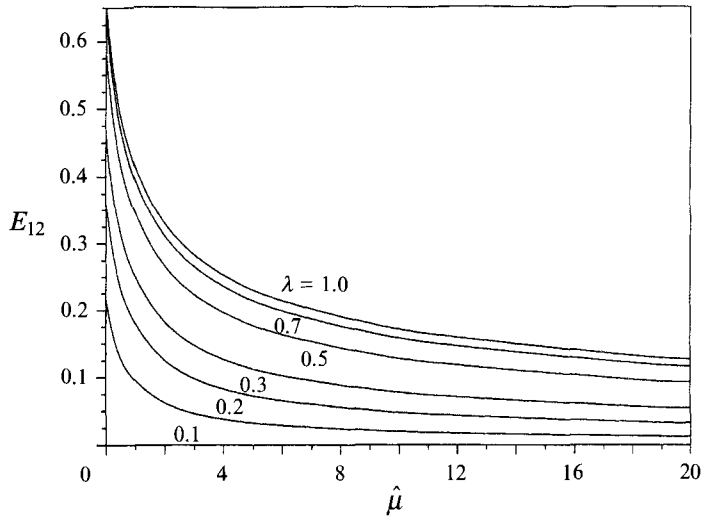

FIGURE 7. The collision efficiency for drops in a uniaxial flow field as a function of the viscosity ratio for various drop size ratios without interdroplet forces.

Using (20), the collision efficiency for uniaxial extensional flow is

$$E_{12} \equiv \frac{J_{12}}{J_{12}^{(0)}} = \frac{1}{\varphi^3(2)}. \tag{26}$$

The calculated collision efficiencies for uniaxial extensional flow as a function of size ratio for different viscosity ratios are shown in figure 6. The collision efficiency E_{12} decreases as the size ratio λ increases, because a smaller drop tends to follow the streamlines of the flow around a larger one. In the limit $\hat{\mu} \to \infty$, corresponding to that of rigid spheres, $E_{12} \to 0$. Figure 7 shows the results for collision efficiency as a function of the viscosity ratio, $\hat{\mu}$. As expected, the collision efficiency decreases as $\hat{\mu}$ increases

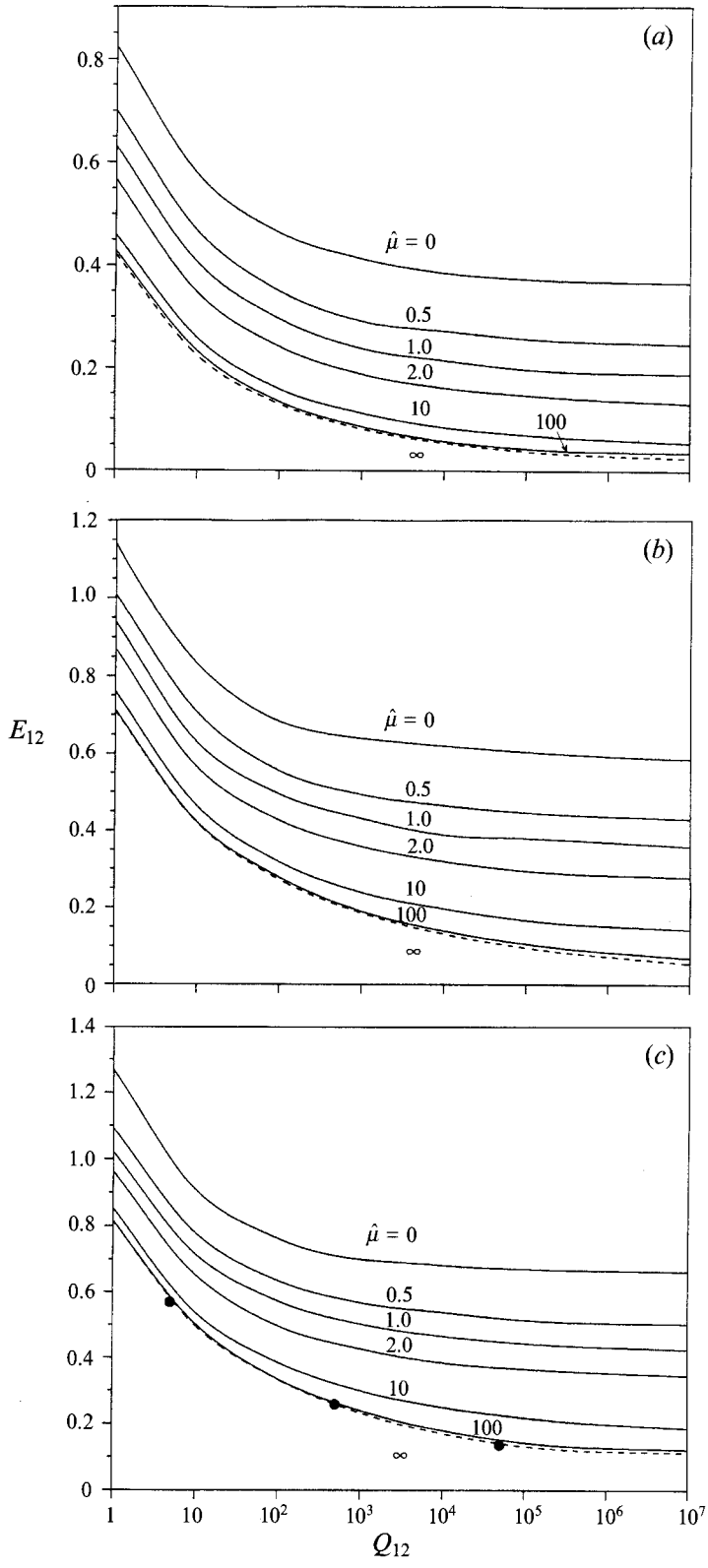

FIGURE 8(*a–c*). For caption see facing page.

because this corresponds to decreasing the interface mobility and internal flow, which leads to a higher hydrodynamic resistance to close approach. The collision efficiency for the inverse flow, namely uniaxial compressional flow, is exactly the same, owing to the reversibility of the linear creeping flow equations.

4.2. *Drop collisions in uniaxial extensional flow with interdroplet forces*

In the presence of van der Waals forces, the trajectory equations must be solved numerically. Since there is no velocity components in the ϕ-direction, as shown in (12), the trajectory equations (10)–(12) are reduced into single equation for $\mathrm{d}s/\mathrm{d}\theta$. The limiting trajectory, which separates collision and non-collision trajectories, is found by selecting an initial condition very near to $\theta = 0$, $s = 2$, and integrating backwards (Feke & Schowalter 1983) using a fourth-order Runge–Kutta–Merson method. In most cases, the integrations were stopped at $s = 10$, and the far-field undisturbed stream functions were then used to compute the upstream interception area.

Typical results for the collision efficiency as a function of Q_{12} are shown in figure 8 for different viscosity and size ratios. As expected, attractive van der Waals forces increase the collision rate. In fact, the collision efficiency becomes larger than unity for very large van der Waals forces, which corresponds to small Q_{12}. In particular, the collision efficiency for $\hat{\mu} \gg 1$ is independent of $\hat{\mu}$ for large attractive forces, but not for small attractive force. The solid circles in figure 8(*c*) represent the calculations by Zeichner & Schowalter (1977) for solid spheres. Our results for $\hat{\mu} = \infty$ agree well with their results, except for low values of Q_{12}. The discrepancy is due to some minor errors in their calculations (Feke 1981).

4.3. *Drop collisions in simple shear flow without interdroplet forces*

When interdroplet forces are neglected, the last term on the right-hand side of (6) is zero. Equations (6)–(8), which describe the relative trajectories for a pair of drops in simple shear flow, then yield the following integrals of the relative trajectories (Batchelor & Green 1972*a*):

$$\bar{x}_3 = \xi_3 \varphi(s), \tag{27}$$

$$\bar{x}_2^2 = \varphi^2(s)\,[\xi_2 + \Psi(s)], \tag{28}$$

where $\bar{x}_i = 2x_i/a_1(1+\lambda)$ for $i = 1, 2, 3$ are the dimensionless coordinates, and ξ_2 and ξ_3 are the constants specifying a particular trajectory. The expression for $\Psi(s)$ is

$$\Psi(s) = \int_s^\infty \frac{\mathscr{B}(s')\,s'\,\mathrm{d}s'}{[1-\mathscr{A}(s')]\,\varphi^2(s')}. \tag{29}$$

Following the work of Zinchenko (1984), we define the following regions in $\boldsymbol{r}$-space ($s > 2$):

$$D_f\colon \quad \bar{x}_2^2 < \varphi^2(s)\,\Psi(s), \tag{30}$$

$$D_t\colon \quad \bar{x}_2^2 + \bar{x}_3^2 \leqslant \varphi^2(s)\left[\frac{4}{\varphi^2(2)} - \Psi(2) + \Psi(s)\right], \tag{31}$$

where D_f is the domain consisting of finite trajectories, and D_t is the region occupied by the trajectories touching the contact surface $r = a_1 + a_2$. There are several types of

FIGURE 8. The collision efficiency as a function of the interdroplet force parameter Q_{12} for drops in a uniaxial extensional flow field with different viscosity ratio $\hat{\mu}$ and size ratios (*a*) $\lambda = 0.2$, (*b*) $\lambda = 0.5$, and (*c*) $\lambda = 1.0$. The solid circles represent the rigid sphere results of Zeichner & Schowalter (1977).

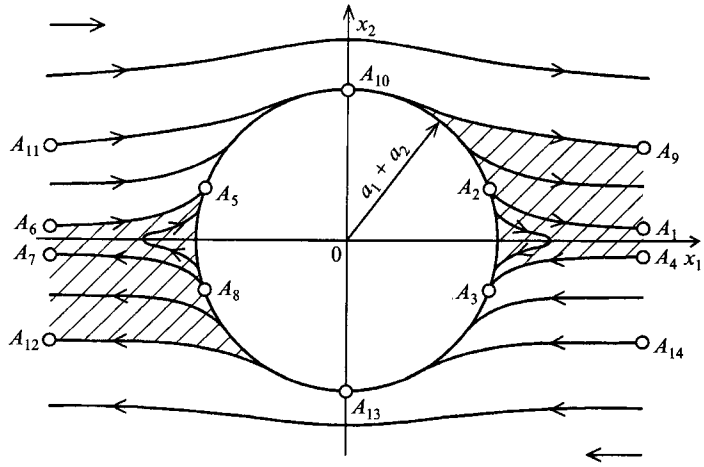

FIGURE 9. A typical pattern of relative trajectories in the $x_3 = 0$ plane.

possible relative trajectories: (i) open trajectories, which do not belong to region $D_f \cup D_t$, are trajectories that arrive from infinity and depart to infinity without reaching the contact sphere $s = 2$; (ii) collision trajectories, forming the region $D_t \backslash D_f$, are the trajectories arriving from infinity at the sphere $s = 2$, or emerging from the sphere $s = 2$ and going to infinity; (iii) semi-closed trajectories, which form the region $D_t \cap D_f$, are trajectories coming from sphere $s = 2$ and returning to it; and (iv) closed trajectories, which form the region $D_f \backslash D_t$.

As mentioned before, $\mathscr{B} \equiv 0$ when $\hat{\mu} = 0$; hence, $\Psi \equiv 0$, and so the region D_f, as defined by (30), vanishes in this case. This may be interpreted as inviscid drops or bubbles not providing enough resistance to relative motion to support finite or closed trajectories. When $\hat{\mu} > 0$, the geometry of the regions D_f and D_t depends on whether the inequality $\varphi^2(2)\,\Psi(2) < 4$ holds. Zinchenko's (1984) calculations show that, in the case of equal-sized drops, there exists some very large viscosity ratio, $\hat{\mu}_c \gg 20$, for which $\varphi^2(2)\,\Psi(2) = 4$. In this study, we found that, owing to the dependence of hydrodynamic interactions on the drop size ratio and on the drop-to-medium viscosity ratio, there exists a critical size ratio, $\lambda_c(\hat{\mu})$, for each viscosity ratio, so that $\varphi^2(2)\,\Psi(2) > 4$ only for $\lambda < \lambda_c$. The critical size ratio is discussed later in more detail. When $\hat{\mu} > \hat{\mu}_c$, the critical size ratio becomes unity, and so the condition $\varphi^2(2)\,\Psi(2) > 4$ holds for all size ratios.

Figure 9 shows a typical pattern of relative trajectories in the $\bar{x}_3 = 0$ plane for $\hat{\mu} < \hat{\mu}_c$ and $\lambda > \lambda_c$. The boundary of the region D_f is formed by rotating the trajectories A_1A_2, A_3A_4, A_5A_6, and A_7A_8 (which all correspond to $\xi_2 = 0$) about the $\bar{x}_2$ axis. It can be shown that, as $s \to \infty$, these trajectories approach the $\bar{x}_1$ axis as $O(s^{-\frac{3}{2}})$. When $\hat{\mu} = 0$, A_1A_2, A_3A_4, A_5A_6, and A_7A_8 tend to the x_1 axis; thus, region D_f vanishes for this case. The pair distribution function in the shaded region in figure 9 equals zero at steady state. The boundary of the region D_t is formed by rotating the trajectories $A_9A_{10}A_{11}$ and $A_{12}A_{13}A_{14}$ (with $\xi_2 = (4/\varphi^2(2)) - \Psi(2)$) about the $\bar{x}_1$ axis and has a circular cross-section area of radius $[(4/\varphi^2(2)) - \Psi(2)]^{\frac{1}{2}}$ as $s \to \infty$. This is the upstream interception area needed to calculate the collision efficiency in the absence of van der Waals forces, and so $\varphi(2)$ and $\Psi(2)$, which are functions of drop size ratio and viscosity ratio, must be calculated.

When $\hat{\mu} > \hat{\mu}_c$, or $\lambda < \lambda_c$, the outer boundary of D_f consists of two separated surfaces of revolution $\xi_2 = 0$ not reaching the sphere $s = 2$, and the region $D_t \subset D_f$ consists of semi-closed trajectories. So, in this case, all of the relative trajectories that start with

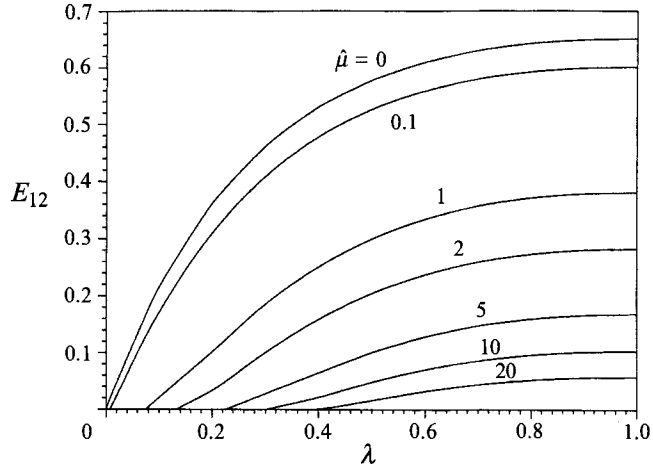

FIGURE 10. The collision efficiency for drops in simple shear flow as a function of the size ratio λ for different viscosity ratios $\hat{\mu}$ without interdroplet forces.

the two drops far apart remain open (no collisions), unless in the presence of other driving forces such as attractive van der Waals forces.

It is seen that the relative trajectories of a pair of fluid drops are different from that of rigid spheres. For two rigid spheres, the only possible trajectories are open trajectories and closed trajectories. The minimum distance between the surface $\xi_2 = 0$ and the contact surface $s = 2$ varies from $4.2 \times 10^{-5} a_1$ for $\lambda = 1$ (Arp & Mason 1977, and Zinchenko 1984) to $0.16 a_1$ for $\lambda = 0$ (Cox, Zia & Mason 1968). So, unlike the drop case, the collision rate is always zero between two rigid spheres, unless in the presence of van der Waals attraction. The integrals in (22) and (29) with $s = 2$ were computed using exact bispherical coordinate solutions and near-field asymptotic expressions as described in Appendices A and B. Note that, for high viscosity ratio $\hat{\mu}$, these integrals are difficult to calculate owing to a significant contribution from the near-field region.

The calculated collision efficiencies between drops of different sizes in a simple shear flow with different values of $\hat{\mu}$ are shown in figure 10. As expected, the collision efficiency decreases with increasing drop viscosity. It is also seen that the collision efficiency is zero when λ is smaller than some critical size ratio for each $\hat{\mu}$. When λ is larger than that value, the collision efficiency increases with increasing size ratio. Figure 11 shows the critical value of the size ratio as a function of the viscosity ratio; this curve demarcates the region for a dispersion to be unstable (collisions possible) and to be stable (collisions not possible) under the action of simple shear flow only. When the viscosity ratio is high enough, the collision efficiency will be zero for all size ratios, and the dispersion is then stable. This prediction is particularly important for controlling the properties of dispersions for practical applications.

Figure 12 shows the results for the collision efficiency for drops in simple shear flow as a function of $\hat{\mu}$ for $\lambda = 0.1$, 0.2, 0.3, 0.5, 0.7, and 1.0. As expected, E_{12} decreases as $\hat{\mu}$ increases because this corresponds to increasing hydrodynamic interactions. For size ratios below unity, the collision rate reaches zero at a finite $\hat{\mu}$, corresponding to the demarcation curve of figure 11. This is in contrast to the uniaxial flow case (see figure 7) in which non-zero collision rates are predicted for all finite λ and $\hat{\mu}$.

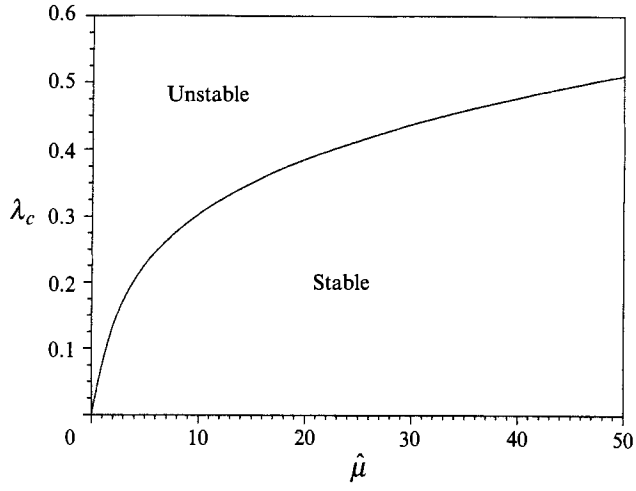

FIGURE 11. The critical size ratio λ_c as a function of the viscosity ratio $\hat{\mu}$, which demarcates two regions: one for the dispersion to be stable (no collisions possible) and the other to be unstable (collision possible) under simple shear flow.

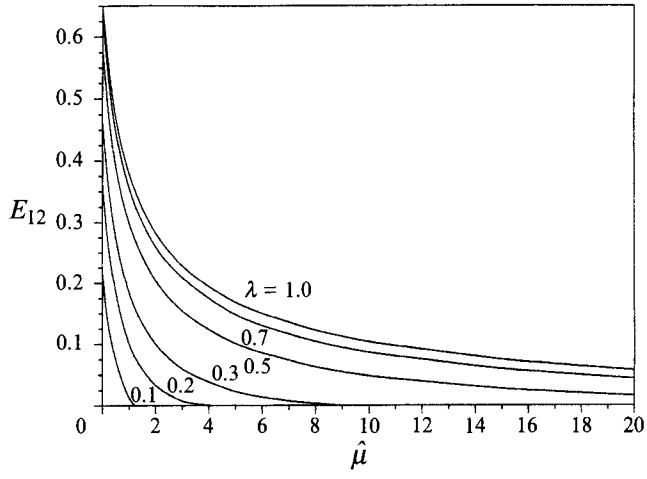

FIGURE 12. The collision efficiency for drops in a simple shear flow field as a function of the viscosity ratio $\hat{\mu}$ for various drop size ratios λ without interdroplet forces.

4.4. *Drop collisions in simple shear flow with interdroplet forces*

With the presence of interparticle forces, the upstream interception area is of irregular shape; thus, the collision efficiencies are more difficult to calculate than when van der Waals forces are absent. In the numerical routine, the three trajectory equations for dr/dt, $d\phi/dt$, and $d\theta/dt$, which describe the time rate of change of the relative position of the drops, are reduced to two equations, $ds/d\phi$ and $d\theta/d\phi$, by eliminating time as the independent variable for drops in simple shear flow. The trajectory equations were integrated numerically using a fourth-order Runge–Kutta–Merson method.

Without interdroplet forces, all collisions occur in the front hemisphere when two drops start from far apart. There may also exist some closed trajectories of drops orbiting around each other under simple shear flow, as discussed before. When attractive van der Waals forces are present, however, drop collisions may occur in the

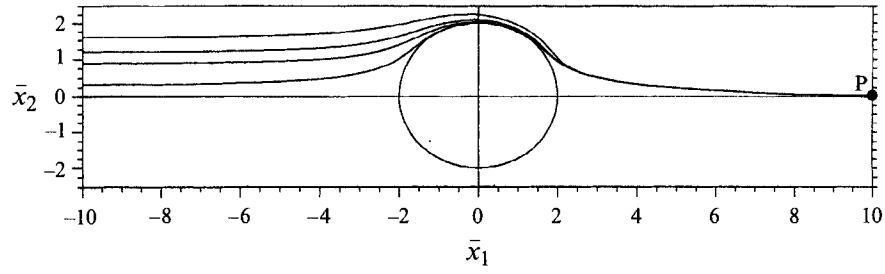

FIGURE 13. Trajectories in simple shear flow in the $(\bar{x}_1, \bar{x}_2)$-plane for a viscosity ratio of $\hat{\mu} = 10$ and a size ratio of $\lambda = 0.5$; the curves represent values of the interdroplet force parameter of $Q_{12} = 1.0$, 10, 10^3, and 10^5, respectively, from top to bottom.

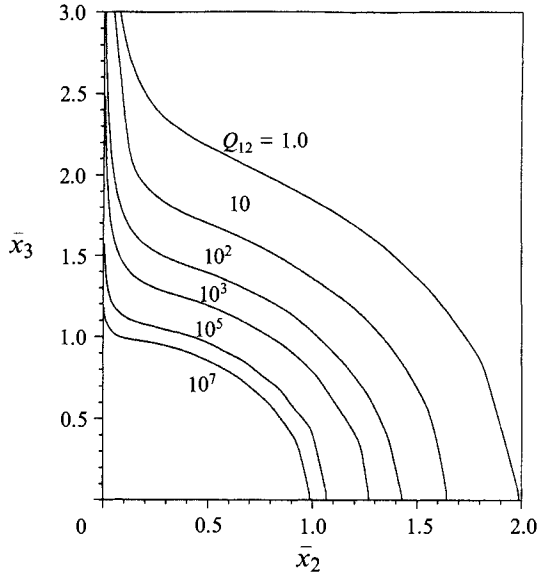

FIGURE 14. The upstream interception area as a function of the interdroplet force parameter Q_{12} for drops in simple shear flow field with viscosity ratio $\hat{\mu} = 10$, and size ratio $\lambda = 1.0$.

rear hemisphere. More interestingly, the drops may undertake multiple circulations around each other before eventually colliding due to the van der Waals attraction. In our trajectory analysis, we include all collision possibilities by employing the backward integration method discussed below. The purpose of this backward integration is to find the limiting trajectory that separates the collision and non-collision trajectories.

It is well known that van der Waals forces for supramicron drops are only important when the drops are very close to each other (Zhang & Davis 1991). When drops are far apart, the hydrodynamic interactions predominate, and the van der Waals forces can be neglected. Based on this, the far downstream part of the set of limiting trajectories with large s should coincide with the boundary of D_f as defined before. A trajectory with its far downstream part outside D_f will depart to infinity. On the other hand, if the far downstream part of a trajectory is inside D_f, this trajectory will eventually come back to collide with the contact surface. The remaining part of the limiting trajectories can be found by integrating the far downstream portion of the trajectories backward starting from the boundary of D_f. This approach was first used by Adler (1981) for the calculation of collision efficiencies for rigid spheres.

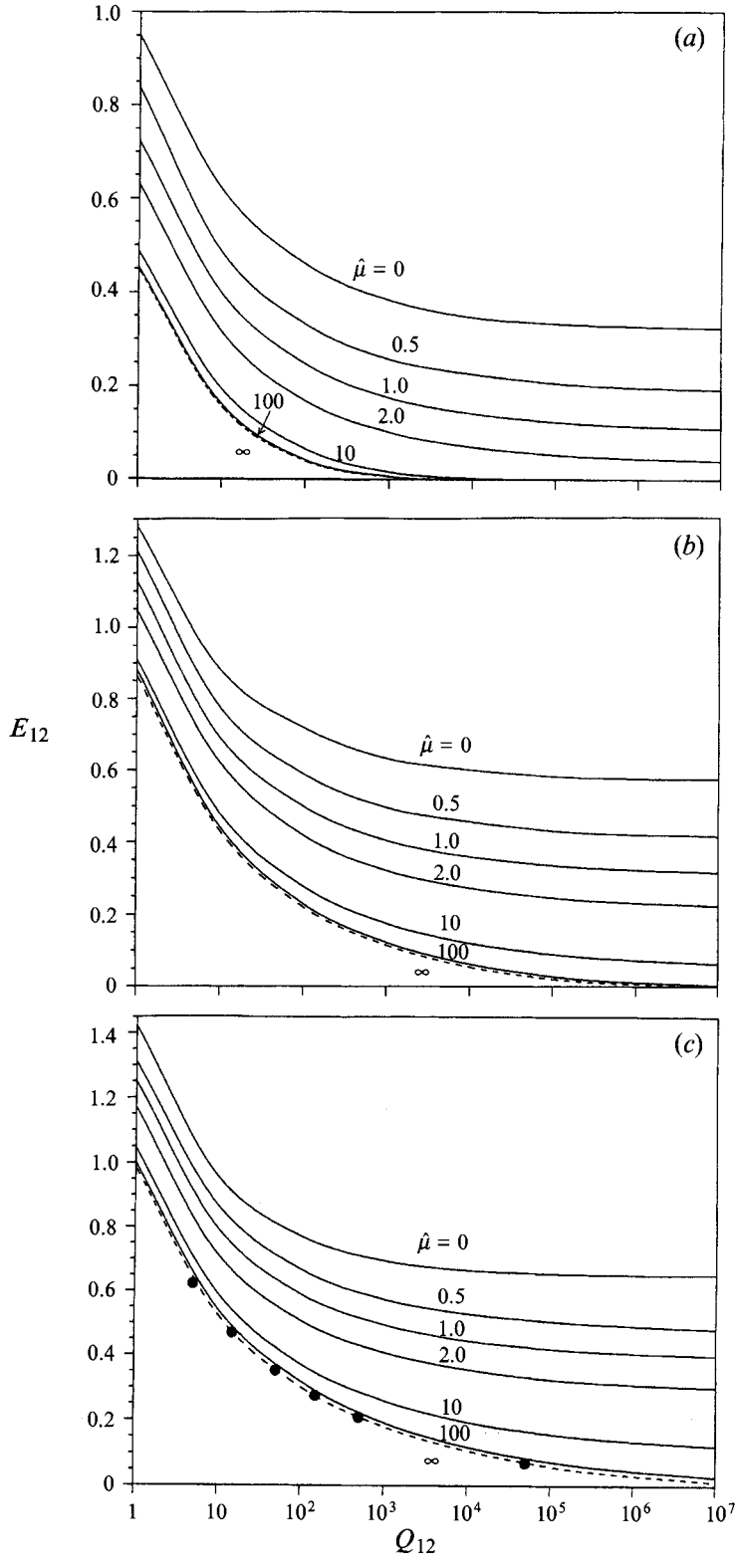

FIGURE 15(*a–c*). For caption see facing page.

In order to locate the boundary of D_f far away from the origin, the far-field expressions for $\mathscr{A}$ and $\mathscr{B}$ are substituted into (27) and (28) to obtain the limiting trajectories far downstream from contact:

$$\bar{x}_3 = \xi_3\left[1+\frac{4}{3}\frac{(2+5\hat{\mu})(1+\lambda^3)}{(1+\hat{\mu})(1+\lambda)^3}\frac{1}{s^3}\right], \tag{32}$$

$$\bar{x}_2^2 = \left(\frac{\bar{x}_3}{\xi_3}\right)^2\left[\xi_2+\frac{32}{2}\frac{\hat{\mu}(2+3\hat{\mu})(1+\lambda^5)+\hat{\mu}(2+5\hat{\mu})\lambda^2(1+\lambda)}{(1+\hat{\mu})(2+3\hat{\mu})(1+\lambda)^5}\frac{1}{s^3}\right]. \tag{33}$$

Figure 13 illustrates this backward integration method for calculating the limiting trajectories in the $(\bar{x}_1, \bar{x}_2)$-plane with $\theta = \frac{1}{2}\pi$ for $\hat{\mu} = 10$, $\lambda = 0.5$, and different Q_{12}. The limiting trajectories are found by backward integration starting from point P calculated by (32) and (33) with $s = 10$ and $\xi_2 = 0$. This backward integration is stopped when the limiting trajectories reach $s = 10$ upstream, and then (32) and (33) are used again to determine the limiting trajectories to upstream infinity. As expected, the upstream offset in the $\bar{x}_2$ direction, as shown in figure 13, increases with increasing van der Waals forces, or correspondingly decreasing Q_{12}.

Starting from $s = 10$ and different initial values of θ according to (32) and (33) with $\xi_2 = 0$, the set of limiting trajectories are obtained that defines the upstream interception area, as shown in figure 14. As expected, the cross-section area is a decreasing function of Q_{12}. Notice that the curves bounding the cross-section area tend to infinity when $\bar{x}_2 \to 0$. The physical reason is that, when $\bar{x}_2 = 0$, there is no relative motion for a pair of drops due to bulk shear flow. Thus, van der Waals forces will pull the drops together even if they start far apart.

The collision efficiency as a function of Q_{12} for different viscosity and size ratios is shown in figure 15. It is seen that the collision efficiency increases with increasing van der Waals attractions (decreasing Q_{12}). Of particular interest are the cases of $\hat{\mu} = 10$ and 100 for $\lambda = 0.2$, for which collisions are impossible in the absence of van der Waals attractions but for which small but non-zero collision efficiencies are obtained with sufficiently strong van der Waals attractions. The solid circles in figure 15(*c*) represent the results of Zeichner & Schowalter (1977) for equal-sized hard spheres; these agree well with the present calculations for $\hat{\mu} = \infty$.

It should be noted that the backward integration method employed is not possible for the bubble case of $\hat{\mu} = 0$. In this case, $\mathscr{B} \equiv 0$, and the region D_f vanishes. In this case, the limiting trajectories are determined by backward integration starting from an initial condition very close to $\phi = 0$ and $s = 2$, and by varying the initial condition on θ from 0 to $\frac{1}{2}\pi$.

5. Conclusions

This work provides quantitative predictions of drop collision rates in simple shear and uniaxial extensional flows. In this study attention is restricted to dilute dispersions of freely suspended drops, as is the case when the drops are neutrally buoyant, or when the dispersion is processed in a reduced-gravity environment. The drops are considered to have clean interfaces which are free of surfactants and charges. In this study, the

FIGURE 15. The collision efficiency as a function of the interdroplet force parameter Q_{12} for drops in a simple shear flow field with different viscosity ratios $\hat{\mu}$ with size ratios (*a*) $\lambda = 0.2$, (*b*) $\lambda = 0.5$, and (*c*) $\lambda = 1.0$. The solid circles represent the rigid-sphere results of Zeichner & Schowalter (1977).

temperature gradients are assumed small, so that thermocapillary effects (Young, Goldstein & Block 1959; Subramanian 1992) are negligible. It is assumed that the drops are sufficiently small that inertia is negligible and that the drops remain spherical. The former requires that the Reynolds number, $Re = \rho\gamma a_1^2/\mu$, is small compared to unity. For typical conditions of $\mu = 0.01$ g cm^{-1} s^{-1}m, $\rho = 1$ g cm^{-3}, and $\gamma = 1$ s^{-1} (Adler 1981; Cox *et al.* 1968), this restriction is met for $a_1 < 300$ μm. Yiantsios & Davis (1991) have shown that the modified capillary number, which is defined as $Ca = \mu\gamma a_1^2/\sigma h_0$, must be small compared with unity in order for the deformation to be small relative to the separation distance, where σ is the interfacial tension and h_0 is the distance separating the drop interfaces at the point of nearest contact. For the above system with $\sigma = 10$ dyne cm^{-1}, this condition is also met for $a_1 < 300$ μm, provided that $h_0 > 0.0003a_1$. Since van der Waals forces are likely to dominate at such small separations (Zhang & Davis 1991), we conclude that the near-contact deformation is not likely to affect the collision rate under these conditions. It is also assumed in the analysis that Brownian motion is negligible. This requires that the Péclet number, $Pe = \gamma a_1^2/D_{12}^{(0)}$, is large compared with unity. For the above system at room temperature, this requires that $a > 1$ μm.

Using a trajectory analysis to follow the relative motion of a pair of drops, theoretical models to determine the collision efficiencies, both with and without interdroplet forces, have been developed. Complete hydrodynamic interaction between two spheres is included in the analysis. It is shown that finite collision rates between non-deforming fluid drops in uniaxial extensional and in simple shear flows are possible in the absence of attractive forces. Collision rates are shown to decrease as the drop size ratio decreases. For drops in simple shear flow, however, it is found that no collision trajectory exists when the size ratio of two interacting drops is small. This implies that the two drops will not collide with each other if they start far apart, unless in the presence of other driving forces which pull them together. Collision rates are also shown to increase as the viscosity ratio decreases due to the decreasing effects of hydrodynamic interactions on drop relative motion.

This research was supported by NASA Grant NAG3-1277, NSF Grant CTS-8914236, and a Cooperation in Applied Science and Technology travel grant from the National Research Council.

Appendix A. Calculation of axisymmetric mobility functions

The method employed for calculating the mobility functions $\mathscr{G}$ and $\mathscr{A}$ for axisymmetric motion of two drops along their line-of-centres is a generalization of the bispherical coordinate solution by Haber, Hetsroni & Solan (1973) and Rushton & Davies (1973) for the motion of two drops along the line-of-centres in a quiescent liquid. The analysis includes an additional axisymmetric pure straining flow far from the particles and has a simpler formalism.

Let ρ, θ, z be a system of cylindrical coordinates associated with Cartesian coordinates x, y, z ($x + iy = \rho\, e^{i\theta}$, see figure 16). The bispherical coordinates ξ, η are introduced as follows:

$$z = \frac{c \sinh\eta}{\cosh\eta - \mu}, \quad \rho = \frac{c \sin\xi}{\cosh\eta - \mu}, \quad \mu = \cos\xi. \tag{A 1}$$

The spheres 1 and 2 of radii a_1 and a_2, respectively, become coordinate surfaces

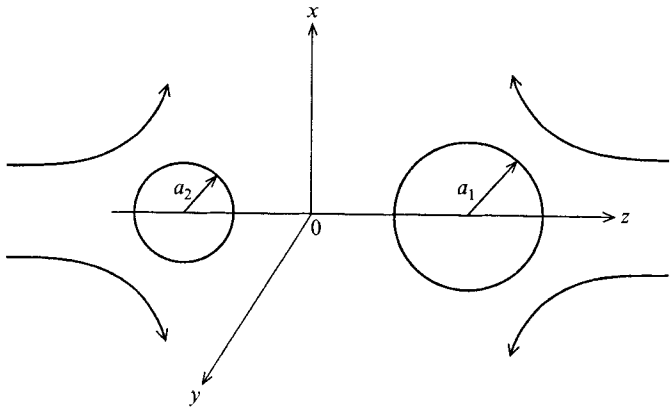

FIGURE 16. Sketch of the coordinate system for two drops.

$\eta = \eta_i = \text{const}$ $(i = 1, 2)$ if the parameters $\eta_1 > 0$, $\eta_2 < 0$, and $c > 0$ are determined from the relations

$$\left.\begin{aligned} \cosh\eta_1 &= \frac{(\lambda+1)[2(\lambda+1)\xi+4+(\lambda+1)^2\xi^2]}{2(\xi+2)(1+\lambda)}, \\ \sinh\eta_2 &= -\sinh\eta_1/\lambda, \quad c = a_1\sinh\eta_1. \end{aligned}\right\} \tag{A 2}$$

Suppose the drops have the velocities V_1, V_2 along the z-axis and are submerged in a pure straining flow

$$\boldsymbol{v}_\infty = (Ex, Ey, -2Ez), \tag{A 3}$$

with E being an arbitrary constant. Using the general solution by Stimson & Jeffrey (1926) for the Stokes' axisymmetrical problem in bispherical coordinates, the stream function ψ inside the drops can be written as

$$\left.\begin{aligned} \psi &= c^2\sqrt{2}(\cosh\eta-\mu)^{-\frac{3}{2}}\sum_{n=1}^{\infty} n(n+1)\,\psi_n(\eta)\,Q_n(\mu), \\ Q_n(\mu) &= \frac{P_{n+1}(\mu)-P_{n-1}(\mu)}{2n+1}, \end{aligned}\right\} \tag{A 4}$$

where $P_n(\mu)$ is the Legendre polynomial of degree n and $\psi_n(\eta)$ is a linear combination of the functions $\exp[\pm(n-\frac{1}{2})\eta]$, $\exp[\pm(n+\frac{3}{2})\eta]$. The regularity of the flows inside the drops implies

$$\left.\begin{aligned} \psi_n^1(\eta) &= A_n\exp[-(n-\tfrac{1}{2})\eta]+B_n\exp[-(n+\tfrac{3}{2})\eta], \\ \psi_n^2(\eta) &= C_n\exp[(n-\tfrac{1}{2})\eta]+D_n\exp[(n+\tfrac{3}{2})\eta], \end{aligned}\right\} \tag{A 5}$$

with A_n, B_n, C_n, and D_n being unknown constants. Here and henceforth the superscripts 1 and 2 mark the values related to the flows inside the spheres 1 and 2, respectively. Employing (A 4) outside the spheres (region e), with $\psi_n(\eta)$ being a combination of $\exp[\pm(n-\frac{1}{2})\eta]$ and $\exp[\pm(n+\frac{3}{2})\eta]$, would yield a flow that vanishes at infinity (Stimson & Jeffrey 1926), and so the unperturbed stream function $\psi_\infty = E\rho^2 z$ should be added to this result. To obtain the bispherical-coordinate representation for ψ_∞, we use the identity (see Stimson & Jeffrey 1926)

$$\tfrac{1}{2}\rho^2 = -c^2\sqrt{2}(\cosh\eta-\mu)^{-\frac{3}{2}}\sum_{n=1}^{\infty} n(n+1)\,R_n(\eta)\,Q_n(\mu), \tag{A 6}$$

where $$R_n(\eta) = \frac{1}{2}\left[\frac{\exp[-(n-\frac{1}{2})|\eta|]}{2n-1} - \frac{\exp[-(n+\frac{3}{2})|\eta|]}{2n+3}\right]. \tag{A 7}$$

Differentiating (A 6) with respect to η yields

$$\psi_\infty = c^2\sqrt{2}\sum_{n=1}^{\infty} n(n+1)\,\psi_n^\infty(\eta)\,Q_n(\mu), \tag{A 8}$$

where $$\psi_n^\infty(\eta) = -2cE\sinh\eta\exp[-(n+\tfrac{1}{2})|\eta|]. \tag{A 9}$$

Thus, (A 4) can be also used for the stream function ψ^e outside the spheres with

$$\psi_n^e(\eta) = E_n\exp[(n-\tfrac{1}{2})(\eta-\eta_1)] + F_n\exp[(n-\tfrac{1}{2})(\eta_2-\eta)] + G_n\exp[(n+\tfrac{3}{2})(\eta-\eta_1)] + H_n\exp[(n+\tfrac{3}{2})(\eta_2-\eta)] + \psi_n^\infty(\eta), \tag{A 10}$$

and E_n, F_n, G_n, and H_n being unknown coefficients.

Using (A 6), the boundary conditions

$$\psi^e = \psi^i = -\tfrac{1}{2}V_i\rho^2 \quad \text{for} \quad \eta = \eta_i, \quad i = 1,2 \tag{A 11}$$

of no-flux across the drop surfaces can be readily written as

$$\psi_n^e(\eta_i) = V_i R_n(\eta_i), \quad i = 1,2 \tag{A 12}$$

and $$\psi_n^i(\eta_i) = V_i R_n(\eta_i), \quad i = 1,2. \tag{A 13}$$

The velocity continuity through the interfaces implies

$$\frac{\mathrm{d}\psi_n^e}{\mathrm{d}\eta} = \frac{\mathrm{d}\psi_n^i}{\mathrm{d}\eta} \quad \text{for} \quad \eta = \eta_i, \quad i = 1,2. \tag{A 14}$$

The expression for the component $e_{\xi\eta}$ of the rate-of-strain tensor at $\eta = \eta_i$ greatly simplifies if calculated via the relative velocity $\boldsymbol{U}^* = \boldsymbol{U} - \boldsymbol{V}_i$ past the sphere, where $\boldsymbol{U}$ is the fluid velocity. Indeed, using the no-flux boundary condition $U_\eta^* = 0$, one can derive

$$e_{\xi\eta} = -\frac{1}{2}\frac{\partial}{\partial\eta}\left[\frac{h^2}{\rho}\frac{\partial\psi^*}{\partial\eta}\right] \quad \text{at} \quad \eta = \eta_i, \tag{A 15}$$

with $h = (\cosh\eta - \mu)/c$ being the metric coefficient. The stream function

$$\psi^* = \psi + \tfrac{1}{2}V_i\rho^2$$

for the relative motion is represented by (A 4), with $\psi_n(\eta)$ being replaced by $\psi_n(\eta) - V_i R_n(\eta)$. Thus, using (A 12), (A 13) and (A 15), the conditions of tangential stress continuity through the interfaces can be written as

$$\frac{\mathrm{d}^2}{\mathrm{d}\eta^2}[\psi_n^e(\eta) - V_i R_n(\eta)] = \hat{\mu}\frac{\mathrm{d}^2}{\mathrm{d}\eta^2}[\psi_n^i(\eta) - V_i R_n(\eta)] \quad \text{for} \quad \eta = \eta_i, \quad i = 1,2. \tag{A 16}$$

Relations (A 12)–(A 14) and (A 16) together with (A 5) and (A 10) form the required linear system of eight equations for eight unknowns: A_n, B_n, C_n, D_n, E_n, F_n, G_n, and H_n. It follows from the work of Stimson & Jeffrey (1926) that the hydrodynamic forces $(F_1)_z$, $(F_2)_z$ acting on the drops take the form

$$\left.\begin{aligned}(F_1)_z &= -8\pi\mu c\sum_{n=1}^{\infty} n(n+1)\{E_n\exp[-(n-\tfrac{1}{2})\eta_1] + G_n\exp[-(n+\tfrac{3}{2})\eta_1]\},\\ (F_2)_z &= -8\pi\mu c\sum_{n=1}^{\infty} n(n+1)\{F_n\exp[(n-\tfrac{1}{2})\eta_2] + H_n\exp[(n+\tfrac{3}{2})\eta_2]\}.\end{aligned}\right\} \tag{A 17}$$

It is not necessary to derive cumbersome analytical expressions for E_n, F_n, G_n, and H_n, since the series (A 17) must be summed numerically. However, a simple and useful step is to analytically exclude the coefficients A_n, B_n, C_n, and D_n from the solution. It follows from the exponential forms (A 5) and (A 7) for $\psi_n^i(\eta)$ and $R_n(\eta)$, respectively, and from the boundary conditions (A 13) that

$$\frac{\mathrm{d}^2}{\mathrm{d}\eta^2}[\psi_n^i(\eta)-V_i R_n(\eta)] = \mp(2n+1)\frac{\mathrm{d}}{\mathrm{d}\eta}[\psi_n^i(\eta)-V_i R_n(\eta)] \quad \text{for} \quad \eta=\eta_i, \tag{A 18}$$

where the upper sign stands for $i=1$, the lower one for $i=2$. Hence, using (A 14), conditions (A 16) can be replaced by

$$\frac{\mathrm{d}^2\psi_n^e}{\mathrm{d}\eta^2}\pm\hat{\mu}(2n+1)\frac{\mathrm{d}\psi_n^e}{\mathrm{d}\eta} = V_i\left[\frac{\mathrm{d}^2R_n}{\mathrm{d}\eta^2}\pm\hat{\mu}(2n+1)\frac{\mathrm{d}R_n}{\mathrm{d}\eta}\right] \quad \text{for} \quad \eta=\eta_i, \tag{A 19}$$

where the upper sign holds for $i=1$, the lower one for $i=2$. Relations (A 12) and (A 19) together with (A 10) constitute the desired system of four equations for four unknowns which is solved numerically for arbitrary n to compute the forces (A 17). Note that the boundary conditions (A 19) directly enable the solid-sphere limit $\hat{\mu}\to\infty$.

Owing to linearity of the problem, the hydrodynamic forces can be decomposed as

$$\left.\begin{aligned}(F_1)_z &= -6\pi\mu a_1[\Lambda_{11}(V_1-V_2)+\Lambda_{12}V_2]-6\pi\mu a_1 rE\frac{(\hat{\mu}+\frac{2}{3})}{(\hat{\mu}+1)}D_1,\\ (F_2)_z &= -6\pi\mu a_2[\Lambda_{21}(V_2-V_1)+\Lambda_{22}V_2]+6\pi\mu a_2 rE\frac{(\hat{\mu}+\frac{2}{3})}{(\hat{\mu}+1)}D_2.\end{aligned}\right\} \tag{A 20}$$

The dimensionless resistance coefficients Λ_{ij} represent the forces acting on the drops moving in a quiescent liquid and have been studied and used previously (see Zinchenko 1982 and the references therein). The dimensionless coefficients D_1 and D_2 are new and represent the forces acting on the drops at rest in the extensional flow (A 3).

The relative mobility $\mathscr{G}$ along the line-of-centres may be expressed in terms of the resistance coefficients Λ_{ij}:

$$\mathscr{G} = \frac{(\hat{\mu}+\frac{2}{3})}{(\hat{\mu}+1)(1+\lambda)}\frac{\Lambda_{12}+\lambda\Lambda_{22}}{(\Lambda_{11}\Lambda_{22}+\Lambda_{21}\Lambda_{12})}. \tag{A 21}$$

According to (3), the relative velocity V_2-V_1 along the line-of-centres of two freely suspended drops in the extensional flow (A 3) takes the form $2Er(1-A)$. On the other hand, this relative velocity can be expressed from (A 20) by equating $(F_1)_z$ and $(F_2)_z$ to zero, yielding

$$1-\mathscr{A} = \frac{1}{2}\frac{(\hat{\mu}+\frac{2}{3})}{(\hat{\mu}+1)}\frac{(D_1\Lambda_{22}+D_2\Lambda_{12})}{(\Lambda_{11}\Lambda_{22}+\Lambda_{21}\Lambda_{12})}. \tag{A 22}$$

The proposed form of the numerical solution enables highly accurate calculation of Λ_{ij}, D_1, D_2, $\mathscr{G}$, and $1-\mathscr{A}$, up to extremely small separations. However, for sufficiently small gaps, the convergene of the series (A 17) is slow, with ultimate divergence when the spheres touch. A significant improvement in the efficiency of coalescence rate calculations is achieved by using near-field asymptotics for $\mathscr{G}$ and $1-\mathscr{A}$. For the singular coefficient Λ_{11}, the three-term asymptotics of Zinchenko (1982) holds:

$$\Lambda_{11}\sim\frac{\pi^2\sqrt{2\hat{\mu}}}{16(1+1/\lambda)^{\frac{3}{2}}}\left[\frac{2}{(1+\lambda)\xi}\right]^{\frac{1}{2}}+\frac{\lambda}{3(1+\lambda)}\left(1-\frac{\hat{\mu}^2}{3}\right)\ln\left[\frac{2}{(1+\lambda)\xi}\right]+C_0, \quad \xi\to 0. \tag{A 23}$$

The parameter C_0 depends on λ and $\hat{\mu}$, and has an explicit but cumbersome analytical expression (Zinchenko 1982). The coefficients Λ_{12}, Λ_{22}, D_1, and D_2 in (A 20) have no singularity when the gap tends to zero, and so for small separations these coefficients can be replaced by their limiting values (marked by an asterisk) for two touching spheres. Explicit integral representations are available for Λ_{12}^* and Λ_{22}^* using the tangent-sphere coordinate solution for drops moving in contact along the line-of-centres (Reed & Morrison 1974). Similar tangent-sphere coordinate solution for two touching drops in the extensional flow (A 3) could be constructed to determine D_1^* and D_2^*. However, a much simpler way to estimate Λ_{12}^*, Λ_{22}^*, D_1^*, D_2^*, and C_0 with sufficient accuracy is exploited in the present work based on using the bispherical coordinate solution for several very small separations (with C_0 being estimated as the difference between the exact value of Λ_{11} and the sum of the first two terms on the right-hand side of (A 23)). These approximations along with the exact reciprocity relation,

$$\lambda_{11}-\lambda\Lambda_{21}=\Lambda_{12}, \tag{A 24}$$

yield the desired near-field asymptotic forms for $\mathscr{G}$ and $1-\mathscr{A}$.

The asymptotic expression (A 23) is not uniformly valid when $\hat{\mu}\to\infty$, i.e. for high viscosity ratio the range of separations where (A 23) is applicable becomes too small. So, for $\hat{\mu}\gg 1$ and $\xi\ll 1$, a different asymptotic form was used:

$$\Lambda_{11}\sim\frac{2\lambda^2}{(1+\lambda)^3}\frac{f(m)}{\xi},\quad m=\frac{1}{\hat{\mu}(1+\lambda)}\left(\frac{2\lambda}{\xi}\right)^{\frac{1}{2}}. \tag{A 25}$$

The function $f(m)$ was calculated numerically by Davis *et al.* (1989) via the solution of the boundary integral equation in the lubrication approximation, and an accurate Padé approximant was found:

$$f(m)=\frac{1+0.402m}{1+1.711m+0.461m^2}. \tag{A 26}$$

Unlike (A 23), the asymptotics (A 25) enables the solid-sphere limit $m\to 0$. On the other hand, it can be shown that, when $m\to\infty$, the asymptotics (A 25) matches (A 23) both in the leading term and in the part of the logarithmic term proportional to $\hat{\mu}^2$, provided that $f(m)$ is calculated exactly. A reasonable way, for a given $\hat{\mu}\gg 1$, to select between the two asymptotic forms (A 23) and (A 25) is to compare the exact values of $\mathscr{G}$ and $1-\mathscr{A}$ with the near-field approximations based either on (A 23) or on (A 25) for a sequence of small separations and choose the form which yields the prescribed accuracy for a wider range of separations.

Appendix B. Calculation of asymmetric mobility functions

Our calculations of the mobility functions $\mathscr{B}$ and $\mathscr{H}$ for asymmetric motion normal to the line-of-centres are based on the extension of Zinchenko's (1980) bispherical coordinate solution for two drops moving normal to the line-of-centres in a quiescent liquid to the case with an additional shear flow,

$$\boldsymbol{U}_\infty=(\gamma z,0,0), \tag{B 1}$$

far from the drops (here and henceforth the coordinate systems are the same as in Appendix A). The cumbersome solution of Zinchenko (1980), subsequently referred to as the work I, is not reproduced here to any extent. Instead, only the necessary

modifications to this solution are listed below. Consider two drops moving with velocities $(V_1, 0, 0)$ and $(V_2, 0, 0)$ and submerged in the unperturbed flow (B 1). The cylindrical velocity components inside and outside the drops are sought in the form (O'Neill & Majumdar 1970)

$$U_\rho = \left(\frac{\rho F}{c} + \chi + \psi\right)\cos\theta, \quad U_\theta = (\chi - \psi)\sin\theta, \quad U_z = \left(\frac{zF}{c} + 2\phi\right)\cos\theta, \tag{B 2}$$

with the bispherical-coordinate representation for the 'potentials' F, χ, ψ, and ϕ being

$$\left.\begin{aligned} F &= (\cosh\eta - \mu)^{\frac{1}{2}} \sin\xi \sum_{n=1}^{\infty} f_n(\eta)\, P_n'(\mu), \\ \phi &= (\cosh\eta - \mu)^{\frac{1}{2}} \sin\xi \sum_{n=1}^{\infty} \varphi_n(\eta)\, P_n'(\mu), \\ \chi &= (\cosh\eta - \mu)^{\frac{1}{2}} \sin^2\xi \sum_{n=1}^{\infty} \chi_n(\eta)\, P_n''(\mu), \\ \psi &= (\cosh\eta - \mu)^{\frac{1}{2}} \sum_{n=1}^{\infty} \psi_n(\eta)\, P_n(\mu). \end{aligned}\right\} \tag{B 3}$$

In order to satisfy the Stokes' equation ($\nabla \times \nabla^2 \boldsymbol{u} = 0$), the functions f_n, φ_n, χ_n, and ψ_n inside drops 1 and 2 are proportional to $\exp[\mp(n+\frac{1}{2})\eta]$, where to avoid singularities the upper sign holds for drop 1, and the lower one for drop 2. Outside the drops, the representation (B 2)–(B 3) with f_n, φ_n, χ_n, and ψ_n being linear combinations of $\exp[\pm(n+\frac{1}{2})\eta]$ yields the fluid velocity vanishing at infinity, so the unperturbed flow (B 1) should be added. Note that (B 2) represents (B 1) with $F = \chi = \phi = 0$, and $\psi = \gamma z$. To obtain the representation (B 3) for $\psi = \gamma z$, we use the generating function for Legendre polynomials:

$$(\cosh\eta - \mu)^{-\frac{1}{2}} = \sqrt{2} \sum_{n=0}^{\infty} \exp[-(n+\tfrac{1}{2})|\eta|]\, P_n(\mu), \tag{B 4}$$

and differentiate (B 4) with respect to η. Using (A 1), we arrive at

$$\gamma z = (\cosh\eta - \mu)^{\frac{1}{2}} \sum_{n=0}^{\infty} \psi_n^{\infty}(\eta)\, P_n(\mu), \tag{B 5}$$

where

$$\psi_n^{\infty}(\eta) = \gamma c \sqrt{2(2n+1)} \exp[-(n+\tfrac{1}{2})|\eta|] \operatorname{sign}\eta. \tag{B 6}$$

The equations of continuity inside and outside the droplets and the boundary conditions can be written in a straightforward manner as a system of 16 difference equations, 12 being of second order, and the rest of fourth order, for 16 unknown sequences of coefficients determining f_n, φ_n, χ_n, and ψ_n in all the three regions. This solution would be very inefficient for small separations. It is remarkable that, as in I, the problem can be reduced to only four difference equations, each of the fourth order. The first step is to proceed from f_n, χ_n, and ψ_n to new functions $\alpha_n(\eta)$, $\beta_n(\eta)$, and $\gamma_n(\eta)$ by the transformation

$$\left.\begin{aligned} \alpha_n &= 5f_n + 2\psi_n - 2(n-1)(n+2)\chi_n, \\ \beta_{n-1} &= -(n-1)f_{n-1} - \psi_{n-1} + (n-2)(n-1)\chi_{n-1}, \\ \gamma_{n+1} &= (n+2)f_{n+1} - \psi_{n+1} + (n+2)(n+3)\chi_{n+1}, \end{aligned}\right\} \tag{B 7}$$

for $n \geqslant 1$. The expressions for α_n, β_n, and γ_n inside the drops can be taken in the form (1.6) of work I. Outside the drops

$$\left.\begin{aligned}
\alpha_n^e(\eta) &= I_n^e \exp[-(n+\tfrac{1}{2})\eta] + J_n^e \exp[(n+\tfrac{1}{2})\eta] + 2\psi_n^\infty(\eta),\\
\beta_n^e(\eta) &= K_n^e \exp[-(n+\tfrac{1}{2})\eta] + L_n^e \exp[(n+\tfrac{1}{2})\eta] - \psi_n^\infty(\eta),\\
\gamma_n^e(\eta) &= M_n^e \exp[-(n+\tfrac{1}{2})\eta] + N_n^e \exp[(n+\tfrac{1}{2})\eta] - \psi_n^\infty(\eta),\\
\varphi_n^e(\eta) &= A_n^e \exp[-(n+\tfrac{1}{2})\eta] + B_n^e \exp[(n+\tfrac{1}{2})\eta],
\end{aligned}\right\} \tag{B 8}$$

with ψ_n^∞ being defined by (B 6).

The results of I can then be readily used to write down the equations for I_n^e, J_n^e, K_n^e, L_n^e, M_n^e, N_n^e, A_n^e, B_n^e, $Z_n^1 = \varphi_n^1(\eta_1) - \varphi_n^e(\eta_1)$ and $Z_n^2 = \varphi_n^2(\eta_2) - \varphi_n^e(\eta_2)$. Namely, $\nabla \cdot \boldsymbol{u} = 0$ inside and outside the drops, the velocity continuity through the interfaces, and the no-flux boundary conditions lead to six equations: (1.8), (1.10), and (1.12) of work I (with δ_i replaced by V_i). This process enables us to explicitly express I_n^e, J_n^e, K_{n-1}^e, L_{n-1}^e, M_{n+1}^e, and N_{n+1}^e via A_m^e, B_m^e, Z_m^1, and Z_m^2, with $n-1 \leqslant m \leqslant n+1$. Inverting (B 7) and using the velocity continuity through the interfaces in the form (1.9) of work I then allows us to express all the functions f_n, φ_n, χ_n, and ψ_n inside and outside the drops in terms of the four basic sequences A_m^e, B_m^e, Z_m^1, and Z_m^2 with $n-2 \leqslant m \leqslant n+2$ (that is the essence of the transformation (B 7)). The tangential stress continuity conditioins take the form (1.16), (1.19) of work I (with $\lambda_i = \hat{\mu}$ and $\delta_i = V_i$), eventually leading to a system of four difference equations, each of fourth order:

$$\sum_{k=-2}^{2} \boldsymbol{T}_n^k \boldsymbol{W}_{n+k} = V_1 \boldsymbol{S}_n^1 + V_2 \boldsymbol{S}_n^2 + \gamma \boldsymbol{U}_n \quad \text{for} \quad n \geqslant 1, \tag{B 9}$$

with

$$\boldsymbol{T}_n^k = 0 \quad \text{for} \quad n+k < 1,$$

and the boundary condition

$$\boldsymbol{W}_n \to 0 \quad \text{as} \quad n \to \infty. \tag{B 10}$$

The unknown vector $\boldsymbol{W}_n$ consists of the components

$$A_n^e \exp[-(n+\tfrac{1}{2})\eta_2], \quad B_n^e \exp[(n+\tfrac{1}{2})\eta_1], \quad Z_n^1, \quad Z_n^2. \tag{B 11}$$

The 4×4 matrices $\boldsymbol{T}_n^k$ and the four-component vectors $\boldsymbol{S}_n^1$ and $\boldsymbol{S}_n^2$ are the same as in work I, whereas the four-component vector $\boldsymbol{U}_n$ arises from the ambient shear flow acting on two drops at rest.

The hydrodynamic forces act only in the x-direction and are presented by the infinite series (2.2) of I (without the factors V), the nth terms of the series being expressed via $\boldsymbol{W}_{n-1}$, $\boldsymbol{W}_n$, $\boldsymbol{W}_{n+1}$, V_1, V_2, and γ using (1.19) of work I. These forces can be decomposed into the parts due to the drop motion in a quiescent liquid and to the case of drops at rest in the shear flow (B 1). Each part is computed as a limit of a recurrent sequence as $n \to \infty$ using (B 9), in the same manner as in I. In particular, inverting the resistance matrix for the motion in a quiescent liquid yields the relative mobility coefficient $\mathscr{H}$. Besides, equating the net hydrodynamic forces to zero, we obtain the relative velocity $V_1 - V_2$ via the shear rate γ, which, according to (3), should be equivalent to $V_1 - V_2 = \gamma r(1 - \frac{1}{2}\mathscr{B})$, thus yielding the function $\mathscr{B}$.

The calculations in double precision on computers with different mantissa length demonstrate a high reserve of accuracy (usually four or more true decimal figures) in calculating $\mathscr{B}$ and $\mathscr{H}$ for size ratios in the range $0.1 \leqslant \lambda \leqslant 10$ and viscosity ratios in the range $\hat{\mu} \leqslant 100$, for separations in the range $\xi \geqslant 2 \times 10^{-4}$. However, for very small separations, the direct computation of $\mathscr{B}$ and $\mathscr{H}$ has slow convergence. According to the numerical results, for fluid spheres the functions $\mathscr{B}(\xi)$ and $\mathscr{H}(\xi)$ approach their

limiting values for touching with an error $O(\xi)$, and so a linear extrapolation can be used for 'moderate' values of $\hat{\mu}$, to considerably increase the efficiency of collision rate calculations, as in Zhang & Davis (1991). The idea of linear extrapolation fails at high viscosity ratio, since for solid spheres $\mathscr{B}(\xi)$ and $\mathscr{H}(\xi)$ approach $\mathscr{B}(0)$, $\mathscr{H}(0)$ with an error $O(|\ln \xi|^{-1})$ (see Batchelor & Green 1972 and Batchelor 1976). However, for high viscosity ratios, the strongly singular van der Waals forces should be usually taken into account, which makes the collision rate calculations only weakly sensitive to the accuracy of hydrodynamic functions at small separations.

REFERENCES

ADLER, P. M. 1981 Heterocoagulation in shear flow. *J. Colloid Interface Sci.* **83**, 106–115.

ARP, P. A. & MASON, S. C. 1977 The kinetics of flowing dispersions VIII. Doublets of rigid spheres (Theoretical). *J. Colloid Interface Sci.* **61**, 21–43.

BATCHELOR, G. K. 1976 Brownian diffusion of particles with hydrodynamic interaction. *J. Fluid Mech.* **74**, 1–29.

BATCHELOR, G. K. & GREEN, J. T. 1972*a* The hydrodynamic interaction of two small freely-moving spheres in a linear flow field. *J. Fluid Mech.* **56**, 375–400.

BATCHELOR, G. K. & GREEN, J. T. 1972*b* The determination of the bulk stress in a suspension of spherical particles to order c^2. *J. Fluid Mech.* **56**, 401–427.

COX, R. G., ZIA, I. Y. & MASON, S. G. 1968 Particle motions in sheared suspensions. XXV. Streamlines around cylinders and spheres. *J. Colloid Interface Sci.* **27**, 7–18.

CURTIS, A. S. & HOCKING, L. M. 1970 Collision efficiency of equal spherical particles in a shear flow. *Trans. Faraday Soc.* **66**, 1381–1390.

DAVIS, R. H. 1984 The rate of coagulation of a dilute polydisperse system of sedimenting spheres. *J. Fluid Mech.* **145**, 179–199.

DAVIS, R. H., SCHONBERG, J. A. & RALLISON, J. M. 1989 The lubrication force between two viscous drops. *Phys. Fluids* A **1**, 77–81.

DERJAGUIN, B. & LANDAU, L. 1941 Theory of the stability of strongly charged lyophobic sols and of the adhesion of strongly charged particles in solution of electrolytes. *Acta. Physiochim.* **14**, 633.

FEKE, D. L. 1981 Kinetics of flow-induced coagulation with weak Brownian diffusion. PhD dissertation, University of Princeton.

FEKE, D. L. & SCHOWALTER, W. R. 1983 The effects of Brownian diffusion in shear-induced coagulation of colloidal dispersions. *J. Fluid Mech.* **133**, 17–35.

FUENTES, Y. O., KIM, S. & JEFFREY, D. J. 1988 Mobility functions for two unequal viscous drops in Stokes flow. Part 1. Axisymmetric motions. *Phys. Fluids* **31**, 2445–2455.

FUENTES, Y. O., KIM, S. & JEFFREY, D. J. 1989 Mobility functions for two unequal viscous drops in Stokes flow. Part 2. Asymmetric motions. *Phys. Fluids* A **1**, 61–76.

HABER, S., HETSRONI, G. & SOLAN, S. 1973 On the low Reynolds number motion of two droplets. *J. Multiphase Flow* **1**, 57–71.

HAMAKER, H. C. 1937 The London–van der Waals attraction between spherical particles. *Physica* 4, 1058.

KIM, S. & ZUKOSKI, C. F. 1990 A model of growth by hetero-coalulation in seeded colloidal dispersions. *J. Colloid Interface Sci.* **139**, 198–212.

LIN, C. J., LEE, K. J. & SATHER, N. F. 1970 Slow motion of two spheres in a shear field. *J. Fluid Mech.* **43**, 35–47.

MERIK, D. H. & FOGLER, H. S. 1984 Gravity-induced floculation. *J. Colloid Interface Sci.* **101**, 72–83.

O'NEILL, M. E. & MAJUMDAR, S. R. 1970 Asymmetrical slow viscous motions caused by the translation or rotation of two spheres. Part I. The determination of exact solutions for any values of the ratio of radii and separation parameters. *Z. Angew. Math. Phys.* **21**, 164–179.

REED, L. D. & MORRISION, F. A. 1974 The slow motion of two touching fluid spheres along their line of centers. *Intl J. Multiphase Flow* **1**, 573–583.

RUSHTON, E. & DAVIES, G. A. 1973 The slow unsteady settling of two fluid spheres along their line of centers. *Appl. Sci. Res.* **28**, 37–61.

RUSSEL, W. B., SAVILLE, D. A. & SCHOWALTER, W. R. 1989 *Colloidal Dispersions*. Cambridge University Press.

SATRAPE, J. V. 1992 Interactions and collisions of bubbles in thermocapillary motion. *Phys. Fluids* A **4**, 1883.

SMOLUCHOWSKI, V. 1917 Versuch einer mathematischen theorie der koagulationskinetik kollider losungen. *Z. Phys. Chem.* **92**, 129–168.

SPIELMAN, L. A. 1970 Viscous interactions in Brownian coagulation. *J. Colloid Interface Sci.* **33**, 562–571.

STIMSON, M. & JEFFREY, G. B. 1926 The motion of two spheres in a viscous fluid. *Proc. R. Soc. Lond.* **111**, 110–116.

SUBRAMANIAN, R. S. 1992 The motion of bubbles and drops in reduced gravity. In *Transport Processes in Bubbles, Drops and Particles* (ed. R. P. Chhabra & D. DeKee), p. 1. Hemisphere.

VALIOULIS, I. A. & LIST, E. J. 1984 Collision efficiencies of diffusing spherical particles: hydrodynamic, van der Waals and electrostatic forces. *Adv. Colloid Interface Sci.* **20**, 1–20.

VEN, T. G. M. VAN DE & MASON, S. G. 1977 The microrheology of colloidal dispersions, VIII. Effects of shear on perikinetic doublet formation. *J. Colloid Polymer Sci.* **255**, 794–804.

VERWAY, E. J. & OVERBEEK, J. TH. G. 1948 *Theory of Stability of Lyophobic Colloids*. Elsevier.

WANG, H. & DAVIS, R. H. 1993 Droplet growth due to Brownian, gravitational, or thermocapillary motion and coalescence in dilute dispersions. *J. Colloid Interface Sci.* **159**, 108–118.

WEN, C.-S. & BATCHELOR, G. K. 1985 The rate of coagulation in a dilute suspension of small particles. *Scientia Sinica* A **28**, 172–184.

YIANTSIOS, S. G. & DAVIS, R. H. 1991 Close approach and deformation of two viscous drops due to gravity and van der Waals forces. *J. Colloid Interface Sci.* **144**, 412–433.

YOUNG, N. O., GOLDSTEIN, T. S. & BLOCK, M. T. 1959 The motion of bubbles in a vertical temperature gradient. *J. Fluid Mech.* **6**, 350–356.

ZEICHNER, G. R. & SCHOWALTER, W. R. 1977 Use of trajectory analysis to study stability of colloidal dispersion in flow fields. *AIChE J.* **23**, 243–254.

ZHANG, X. & DAVIS, R. H. 1991 The collisions of small drops due to Brownian and gravitational motion. *J. Fluid Mech.* **230**, 479–504.

ZHANG, X. & DAVIS, R. H. 1992 The collision rate of small drops due to thermocapillary migration. *J. Colloid Interface Sci.* **152**, 548–561.

ZHANG, X., WANG, H. & DAVIS, R. H. 1993 Collective effects of temperature gradients and gravity on droplet coalescence. *Phys. Fluids* A **5**, 1602–1613.

ZINCHENKO, A. Z. 1980 The slow asymmetric motion of two drops in a viscous medium. *Prikl. Matem. Mekhan.* **44**, 30–37.

ZINCHENKO, A. Z. 1982 Calculation of the effectiveness of gravitational coagulation of drops with allowance for internal circulation. *Prikl. Matem. Mekhan.* **46**, 72–82.

ZINCHENKO, A. Z. 1983 Hydrodynamic interaction of two identical liquid spheres in linear flow field. *Prikl. Matem. Mekhan.* **47**, 56–63.

ZINCHENKO, A. Z. 1984 Effect of hydrodynamic interactions between the particles on the rheological properties of dilute emulsions. *Prikl. Matem. Mekhan.* **47**, 56–63.